**Defense Threat Reduction Agency**
**8725 John J. Kingman Road, MS**
**6201 Fort Belvoir, VA 22060-6201**

**DTRA-TR-16-7**

TECHNICAL REPORT

# Debris Hazards Due to Overloaded Conventional Construction Facades



December 2015

HDTRA1-14-C-0001

Bryan Bewick et al.

Prepared by:
Protection Engineering Consultants LLC
14144 Trautwein Rd
Austin, TX 78737

DESTRUCTION NOTICE:

Destroy this report when it is no longer needed.
Do not return to sender.

PLEASE NOTIFY THE DEFENSE THREAT REDUCTION AGENCY, ATTN: DTRIAC/ J9STT, 8725 JOHN J. KINGMAN ROAD, MS-6201, FT BELVOIR, VA 22060-6201, IF YOUR ADDRESS IS INCORRECT, IF YOU WISH IT DELETED FROM THE DISTRIBUTION LIST, OR IF THE ADDRESSEE IS NO LONGER EMPLOYED BY YOUR ORGANIZATION.

# REPORT DOCUMENTATION PAGE

*Form Approved*
*OMB No. 0704-0188*



| **1. REPORT DATE** *(DD-MM-YYYY)* | **2. REPORT TYPE** | **3. DATES COVERED** *(From - To)* |
|---|---|---|
| 00-12-2015 | Technical | August 13, 2014 - August 13, 2015 |

**4. TITLE AND SUBTITLE**

Debris Hazards Due to Overloaded Conventional Construction Facades

**5a. CONTRACT NUMBER**

HDTRA1-14-C-0001

**5b. GRANT NUMBER**

**5c. PROGRAM ELEMENT NUMBER**

**6. AUTHOR(S)**

Bryan Bewick
Greg Rolater
Mohsen Sanai
Adam Ziemba

**5d. PROJECT NUMBER**

**5e. TASK NUMBER**

**5f. WORK UNIT NUMBER**

**7. PERFORMING ORGANIZATION NAME(S) AND ADDRESS(ES)**

Protection Engineering Consultants LLC, 14144 Trautwein Rd, Austin, TX 78737
SRI International, 333 Ravenswood Ave, Menlo Park, CA 94025

**8. PERFORMING ORGANIZATION REPORT NUMBER**

**9. SPONSORING / MONITORING AGENCY NAME(S) AND ADDRESS(ES)**

Defense Threat Reduction Agency
8725 John J. Kingman Road STOP 6201
Fort Belvoir, VA 22060

**10. SPONSOR/MONITOR'S ACRONYM(S)**

DTRA

**11. SPONSOR/MONITOR'S REPORT NUMBER(S)**

DTRA-TR-16-7

**12. DISTRIBUTION / AVAILABILITY STATEMENT**

Distribution Statement A. Approved for public release; distribution is unlimited.

**13. SUPPLEMENTARY NOTES**

**14. ABSTRACT**

Present results for experiments involving conventional façade materials (glass, concrete, and masonry) that have been overloaded to generate debris data at the structural and material levels. The material level samples have been loaded at high pressures using a small diameter shock tube to generate fragmentation at high strain rates. The structural level experiments include full-scale wall components and windows that have been overloaded in a large diameter shock tube at lower strain rates in order to generate structural level fragmentation.

**15. SUBJECT TERMS**

blast, fragmentation, concrete, masonry, debris

| **16. SECURITY CLASSIFICATION OF:** | | | **17. LIMITATION OF ABSTRACT** | **18. NUMBER OF PAGES** | **19a. NAME OF RESPONSIBLE PERSON** |
|---|---|---|---|---|---|
| **a. REPORT** | **b. ABSTRACT** | **c. THIS PAGE** | SAR | 36 | Capt. Paul Clement |
| Unclassified | Unclassified | Unclassified | | | **19b. TELEPHONE NUMBER** *(include area code)* 703-767-4035 |

# UNIT CONVERSION TABLE

## U.S. customary units to and from international units of measurement*

| U.S. Customary Units | Multiply by → / ← Divide by† | | International Units |
|---|---|---|---|
| **Length/Area/Volume** | | | |
| inch (in) | 2.54 | $\times 10^{-2}$ | meter (m) |
| foot (ft) | 3.048 | $\times 10^{-1}$ | meter (m) |
| yard (yd) | 9.144 | $\times 10^{-1}$ | meter (m) |
| mile (mi, international) | 1.609 344 | $\times 10^{3}$ | meter (m) |
| mile (nmi, nautical, U.S.) | 1.852 | $\times 10^{3}$ | meter (m) |
| barn (b) | 1 | $\times 10^{-28}$ | square meter ($m^2$) |
| gallon (gal, U.S. liquid) | 3.785 412 | $\times 10^{-3}$ | cubic meter ($m^3$) |
| cubic foot ($ft^3$) | 2.831 685 | $\times 10^{-2}$ | cubic meter ($m^3$) |
| **Mass/Density** | | | |
| pound (lb) | 4.535 924 | $\times 10^{-1}$ | kilogram (kg) |
| unified atomic mass unit (amu) | 1.660 539 | $\times 10^{-27}$ | kilogram (kg) |
| pound-mass per cubic foot (lb $ft^{-3}$) | 1.601 846 | $\times 10^{1}$ | kilogram per cubic meter (kg $m^{-3}$) |
| pound-force (lbf avoirdupois) | 4.448 222 | | newton (N) |
| **Energy/Work/Power** | | | |
| electron volt (eV) | 1.602 177 | $\times 10^{-19}$ | joule (J) |
| erg | 1 | $\times 10^{-7}$ | joule (J) |
| kiloton (kt) (TNT equivalent) | 4.184 | $\times 10^{12}$ | joule (J) |
| British thermal unit (Btu) (thermochemical) | 1.054 350 | $\times 10^{3}$ | joule (J) |
| foot-pound-force (ft lbf) | 1.355 818 | | joule (J) |
| calorie (cal) (thermochemical) | 4.184 | | joule (J) |
| **Pressure** | | | |
| atmosphere (atm) | 1.013 250 | $\times 10^{5}$ | pascal (Pa) |
| pound force per square inch (psi) | 6.984 757 | $\times 10^{3}$ | pascal (Pa) |
| **Temperature** | | | |
| degree Fahrenheit ($^oF$) | $[T(^oF) - 32]/1.8$ | | degree Celsius ($^oC$) |
| degree Fahrenheit ($^oF$) | $[T(^oF) + 459.67]/1.8$ | | kelvin (K) |
| **Radiation** | | | |
| curie (Ci) [activity of radionuclides] | 3.7 | $\times 10^{10}$ | per second ($s^{-1}$) [becquerel (Bq)] |
| roentgen (R) [air exposure] | 2.579 760 | $\times 10^{-4}$ | coulomb per kilogram (C $kg^{-1}$) |
| rad [absorbed dose] | 1 | $\times 10^{-2}$ | joule per kilogram (J $kg^{-1}$) [gray (Gy)] |
| rem [equivalent and effective dose] | 1 | $\times 10^{-2}$ | joule per kilogram (J $kg^{-1}$) [sievert (Sv)] |

*Specific details regarding the implementation of SI units may be viewed at http://www.bipm.org/en/si/.

†Multiply the U.S. customary unit by the factor to get the international unit. Divide the international unit by the factor to get the U.S. customary unit.

# Debris Hazards Due to Overloaded Conventional Construction Facades

**Bryan Bewick, PhD, PE[1*], Greg Rolater[1], Mohsen Sanai[2], Adam Ziemba[2]**

[1*] *Protection Engineering Consultants, 14144 Trautwein Rd, Austin, TX, USA 78737.*
*(bbewick@protection-consultants.com)*
[2] *SRI International, Menlo Park, CA, USA*

## Abstract

Large blast events will fail building components, such as the façade and supporting structure. Facades present the largest loading surface, are relatively weak, and will fail first and most violently when subjected to blast loads. The range of façade and structural damage extends from complete brisance near ground zero to distances at which the structure survives but the façade fails, and from the end of that range to distances at which the façade and structure are undamaged. For both ranges, the failure of the façade materials presents collateral damage hazards to buildings. This work will present results for experiments involving conventional façade materials (glass, concrete, and masonry) that have been overloaded to generate debris data at the structural and material levels. The material level samples have been loaded at high pressures using a small diameter shock tube to generate fragmentation at high strain rates. The structural level experiments include full-scale wall components and windows that have been overloaded in a large diameter shock tube at lower strain rates in order to generate structural level fragmentation. Results of the experiments and a discussion of the distribution parameters are presented.

*Keywords*: Blast, fragmentation, concrete, masonry, debris.

## INTRODUCTION

The response of blast loaded facades is a function of the pressure and impulse. Higher overpressures can produce smaller fragment sizes due to immediate overloading of the façade materials. Smaller overpressures will result in flexural façade response and fracture resulting from excessive deflections. Debris generation involves multiple length scales, which have been separated into two overlapping regimes termed the materials level (small fragments) and the structural level (structural components). Figure 1 illustrates the overlap of the two regimes.

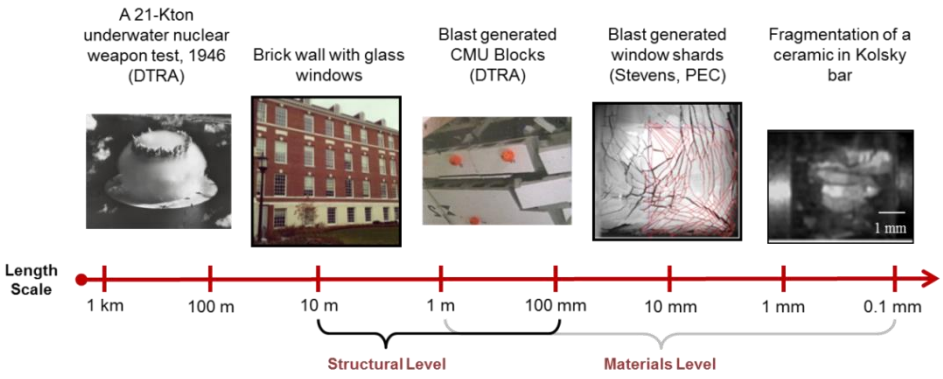


**Figure 1.** Scale of structural and materials level modeling**.**

Because there is no clear transition between these two length domains, and because many blast-loaded facades will exhibit responses in both domains concurrently, efforts have been made to perform experiments at both the material and structural scales. The current paper focuses mainly on the material level experimental work.

## TESTING OVERVIEW

Two test series were performed; material level fragmentation was induced using high-pressure/short-duration tests on small test samples, and structural level fragmentation experiments included low-pressure/long-duration loads on full-scale structural components. The current paper focuses on the high-pressure/short-duration experiments.

### Small Diameter Shock Tube Experiments

The objective of the small diameter shock tube testing was to obtain experimental data for the mass and speed of façade debris generated by high pressure, short duration blast loads. The objective of the experiments were to generate fragmentation data specific to concrete, glass, and concrete masonry. It was also desired to produce data for which the state of stress and strain rates could be estimated. There were two sets of experiments. Figure 2 shows the test setup for the first test series. 40.6-cm (16") square plate samples were placed at the end of the shock tube simply supported by a plate with a 35.6-cm (14") circular opening (sample bears against the support). The concrete and masonry samples were 50.8-cm (2") thick while the glass samples were 6.35-mm (¼") thick.

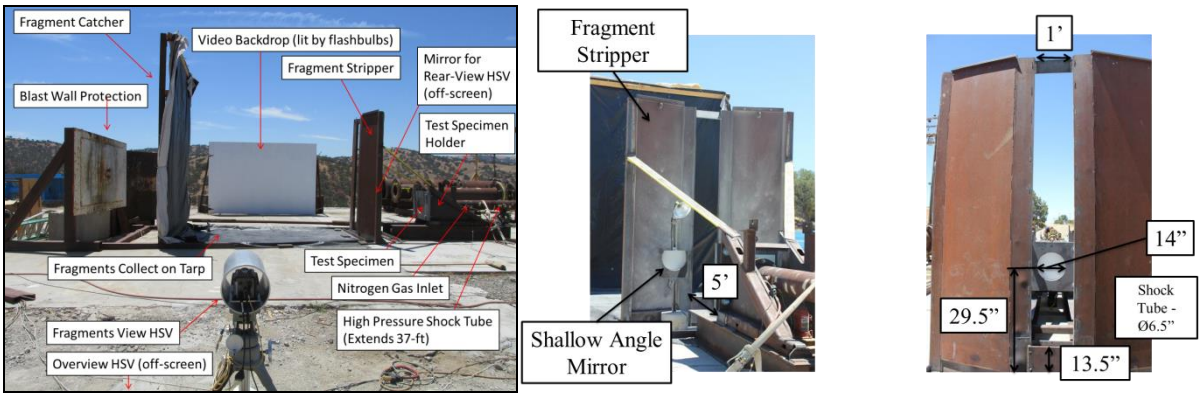


**Figure 2.** Small diameter shock tube series 1 experiment setup

A fragment stripper (Figure 2) allowed only a subset of fragments that were projected out from the sample at an angle less than 5° to pass through. A catcher system allowed for physical collection of the fragments, and high speed video (HSV) was also used to collect data on the fragments. An additional rear view HSV was used to capture the fracture pattern of the samples as they fail. This is useful for two reasons; 1) to show the fracture pattern for comparing with modeling work and 2) the rear view video can be used as an additional way to get fragment size specifically for the glass samples.

The second series of tests were performed with an emphasis on collecting as much of the original sample mass as possible. This was done by rearranging the test setup such that the fragment stripper was removed and the soft capture system was moved closer to the end of the shock tube to trap all of the projectile fragments within the soft capture system. The revised setup eliminated the ability to use the camera setup to capture fragment velocities, but instead placed an emphasis on a higher percentage of mass collection. Figure 3 shows the setup for the second series of experiments. A layered system of Kevlar blanket and carpet was used to capture fragments that flew out of the shock tube at an angle less than 30°.

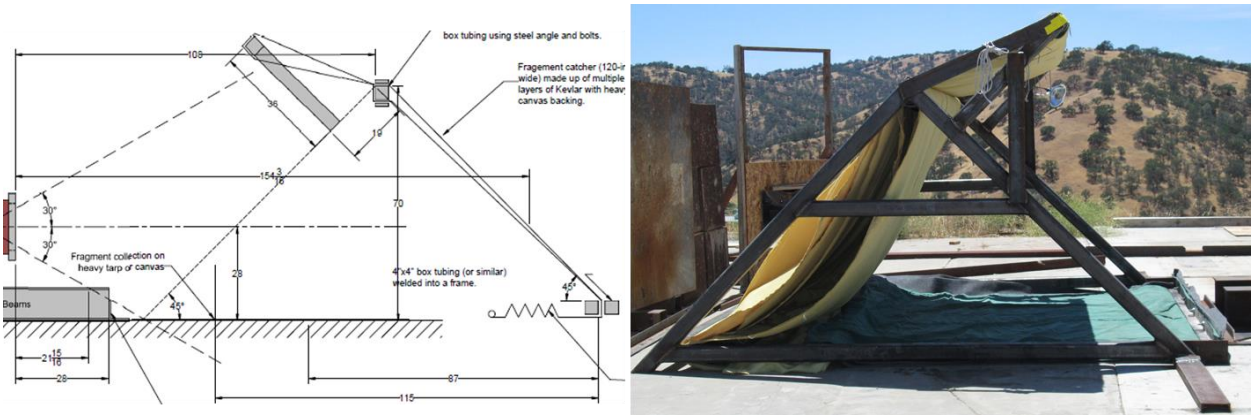


**Figure 3.** Small diameter shock tube series 2 experiment setup

A total of 24 tests with material targets comprising seven masonry targets, six precast concrete targets, and ten glass targets were completed. An additional test was performed with a steel plate bolted at the end of the shock tube to obtain a reference pressure if the target remained intact and did not shatter. Table 1 summarizes the key information for these tests. The test loads were chosen based on preliminary simulations that were completed in LS-DYNA where loads were applied to samples and strain rates were tracked in the model. Figure 4 shows the preliminary simulations defining strain rate and a typical pressure history for the loading type. Figure 5 shows the initial fracture pattern for the different types of materials as the samples break up into smaller fragments.

**Table 1.** High pressure shock tube tests

| *Test* | *Sample* | *Pressure (psi)* | *Impulse (psi-msec)* |
|---|---|---|---|
| **3** | Masonry | 1,259.3 | 2,909 |
| **4** | Masonry | 3,603.7 | 5,514 |
| **5** | Concrete | 1,432.2 | 2,096 |
| **6** | Concrete | N/A* | N/A* |
| **7** | Masonry | 1,347.3 | 1,932 |
| **8** | Concrete | 2,972.5 | 3,264 |
| **9** | Concrete | 2,932.6 | 3,267 |
| **10** | Masonry | 3,167.4 | 4,054 |
| **11** | Steel (Fixed) | 1,775.5 | 4,624 |
| **12** | Masonry | 2,782.3 | 4,009 |
| **13** | Glass | 477.6 | 666.7 |
| **14** | Glass | 235.4 | 340.2 |
| **15** | Glass | 223.9 | 325.6 |
| **16** | Glass | 485.5 | 639.6 |
| **22** | Glass | 223 | 395 |
| **23** | Glass | 407 | 648 |
| **24** | Glass | 440 | 634 |
| **25** | Glass | 2442 | 5326 |
| **29** | Concrete | 542 | 1112 |
| **30** | Concrete | 531 | 1103 |
| **31** | Masonry | 557 | 1083 |
| **32** | Masonry | 587 | 1123 |
| **33** | AN Glass | 435 | 687 |
| **34** | AN Glass | 421 | 710 |

N/A* - Full or partial loss of instrumentation test data

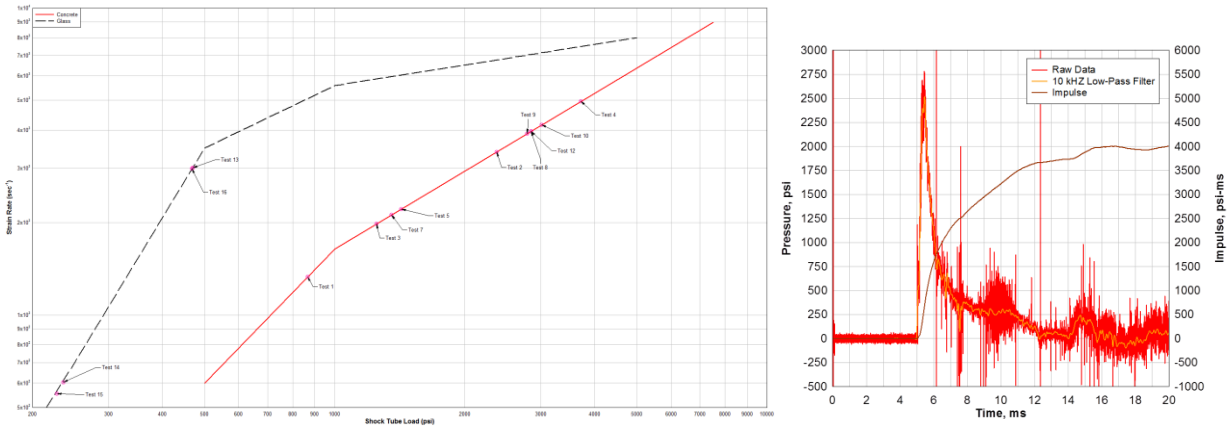


*a* *b*

**Figure 4.** a) Simulated material strain rates based on peak pressure load and b) typical pressure history (test 12 data)

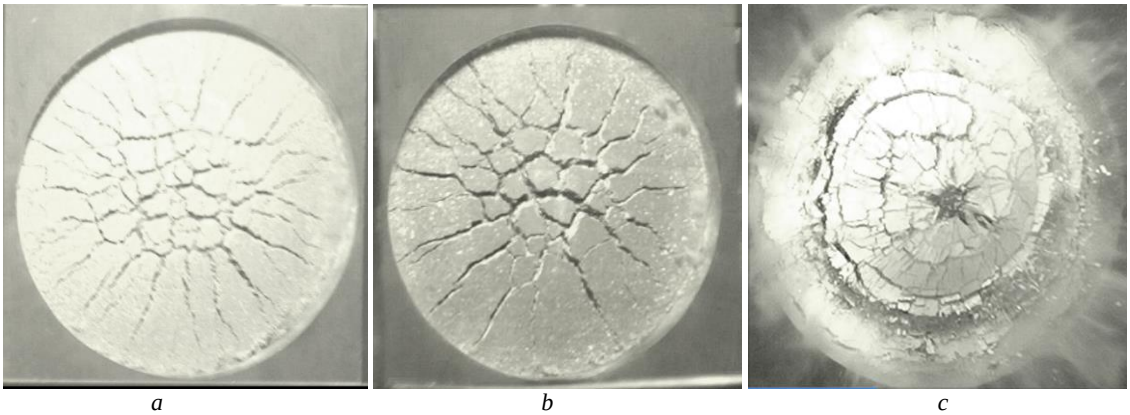

*a* *b* *c*

**Figure 5.** Rear view capture of fracture for a) masonry (test 4), b) concrete (test 8), and c) glass (test 14)

## Debris Distribution Analysis

Distributions for mass and velocity were developed using three approaches to collecting the data; 1) from physical collection of fragments, 2) videographic analysis of side-view HSV, and 3) videographic analysis of rear-view HSV. Fragments which landed in the fragment collection area (Figure 1) were collected and later analysed. The fragments were run through sieves and separated into size groups. Each group was laid out and the SigmaScan Pro software was used to provide a fragment count and the associated area for each individual fragment. The overall mass of each sieve size could then be separated out to a mass for each individual fragment. Figure 6 shows the original and processed image from the no. 4 sieve size (4.75-mm mesh size) for the test 23 fragments.

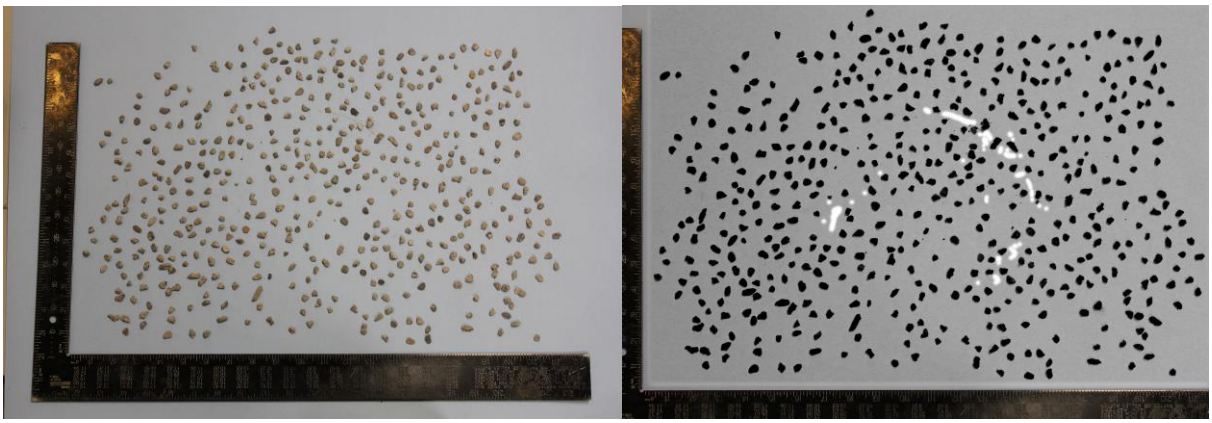

**Figure 6.** Sieve no. 4 SigmaScan data for test 23

The side-view HSV was used to develop velocity and mass data for the tests. PEC's Frag Track software was used to capture the fragment sizes and velocities. The video analysis algorithm searches for closed surface that has an associated velocity gradient all the way around the closed surface. The fragments are then tracked from frame to frame and velocities and sizes can be calculated based on pixel counts. Figure 7 illustrates the fragments being detected and then the trajectory being tracked across the video area. This is a technique that has been used successfully in past efforts for ballistic glass (Barsotti, 2010).

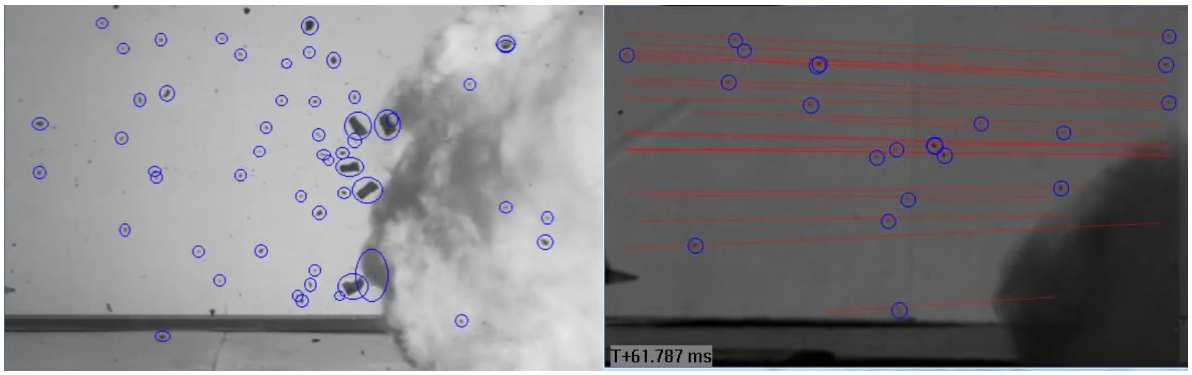


**Figure 7.** Frag Track fragment detections and fragment trajectory tracking

An additional analysis was performed using the rear video for the glass samples. Selected frames were analysed using the SigmaScan Pro software. The frames were pre-processed to subtract the background and outline the fragments monochromatically. Figure 8 shows the progression of the image analysis technique. The last frame shows the delineation of each individual fragment. The technique has been used successfully previously for glass shard flyout models (Stevens, 2002).

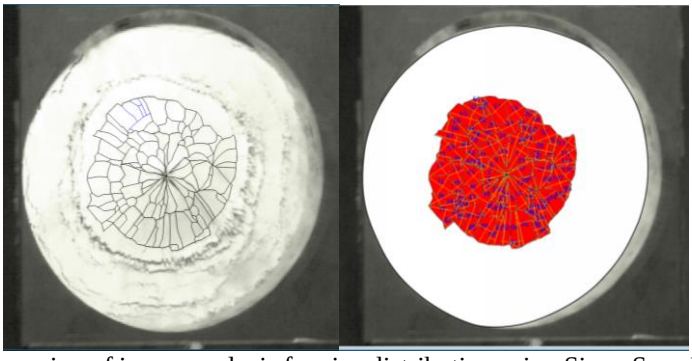

**Figure 8.** Progression of image analysis for size distribution using SigmaScan Pro rear video

## RESULTS

Table 2 shows the amount of mass collected from the subset of fragments which went through the fragment stripper setup. As expected, the weights collected and viewed by the Frag Track algorithm are quite a bit less than the original mass of the sample. This is due to the fragment stripper blocking fragments and from fragments which fell at the base of the shock tube or rebounded in the opposite direction due to boundary conditions. The collected mass is a small portion of the original, but it represents the fragments which are moving with the fastest velocities in the most direct line away from the failing sample. Figure 9 shows an overlay of the mass histograms as developed based on the sieve data and the video analysis. The overlap varies from test to test, but in general the lower limitation of the video analysis was determined to be approximately 0.5-g (0.00112-lb).

**Table 2.** Comparison of sample masses in distribution sets

| *Test* | *Sample* | *Mass (lb)* | *Collected Weight (lb)* | *% of Oringinal Plate Weight* | *Video Tracked Weight (lb)* | *% of Original Plate Weight* |
|---|---|---|---|---|---|---|
| **3** | Masonry | 39.5 | 4.12 | 10% | 1.98 | 5% |
| **4** | Masonry | 40.65 | 1.53 | 4% | 1.36 | 3% |
| **5** | Concrete | 40.2 | 5.30 | 13% | 1.67 | 4% |
| **6** | Concrete | 40.95 | 1.76 | 4% | 1.21 | 3% |
| **7** | Masonry | 39.75 | 4.12 | 10% | 1.76 | 4% |
| **8** | Concrete | 40.9 | 2.56 | 6% | 3.31 | 8% |
| **9** | Concrete | 38.5 | 3.08 | 8% | 1.41 | 4% |
| **10** | Masonry | 40.1 | 1.99 | 5% | 0.6 | 1% |
| **12** | Masonry | 40.55 | 1.93 | 5% | 1.22 | 3% |
| **13** | Glass | 5.2 | 0.48 | 9% | 0.39 | 8% |
| **14** | Glass | 5.2 | 0.72 | 14% | 1.1 | 21% |
| **15** | Glass | 5.2 | 0.72 | 14% | 0.58 | 11% |
| **16** | Glass | 5.15 | 0.50 | 10% | 0.99 | 19% |
| **22** | Glass | 5.15 | 2.31 | 45% | N/A | N/A |
| **23** | Glass | 5.15 | 2.22 | 43% | N/A | N/A |
| **24** | Glass | 5.15 | 2.10 | 41% | N/A | N/A |
| **25** | Glass | 5.15 | 0.34 | 6% | N/A | N/A |
| **29** | Concrete | 40.95 | 16.6 | 40% | N/A | N/A |
| **30** | Concrete | 42.25 | 19.6 | 46% | N/A | N/A |
| **31** | Masonry | 38.15 | 16.1 | 42% | N/A | N/A |
| **32** | Masonry | 36.4 | 14.7 | 40% | N/A | N/A |
| **33** | AN Glass | 5.3 | 2.18 | 41% | N/A | N/A |
| **34** | AN Glass | 5.3 | 2.42 | 46% | N/A | N/A |

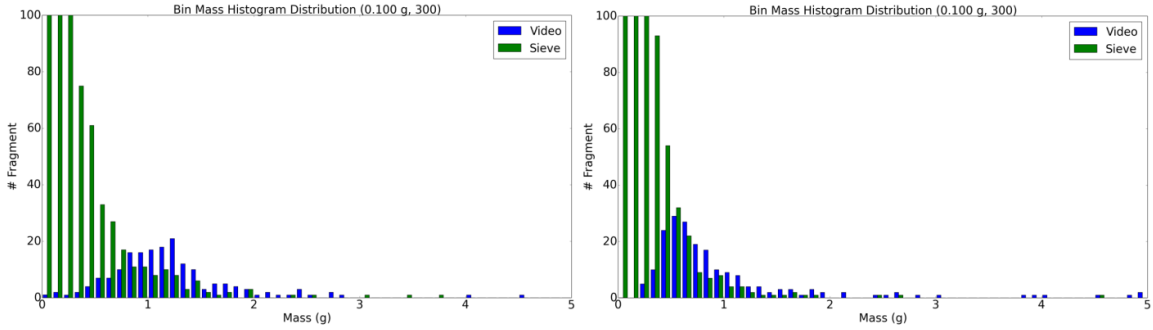


*Test 3* *Test 4*

**Figure 9.** Masonry mass distribution histograms for tests 3 and 4

## Approach to Developing Distributions

The histograms for velocity, mass, and size were normalized and statistical fits were made to the normalized probability distribution functions (PDF). Based on analysis of the cumulative fragment number plots, it was determined that a combined modified Weibull function and power law fit the distributions for the PDFs describing both the mass and velocity distributions. The modified Weibull distribution fit applies to the small fragments which are associated with the middle of the test samples where high rate fragmentation is occurring. The power law distribution fits the larger fragments and generally represents the fragmentation that occurs around the perimeter of the supported test sample. Other fits were considered including the power law, exponential, and a linear distribution for velocity. Equation 1 shows the general form of the modified Weibull PDF distribution. Equation 2 shows the equation for the power law distribution fit.

$$f\left(s/\bar{s}\right) = \frac{b}{a\,\Gamma\left(g/b\right)}\left(\frac{s/\bar{s}}{a}\right)^{g-1} e^{-\left(\frac{s/\bar{s}}{a}\right)^{b}} \tag{1}$$

$$\begin{cases} 1-\left(\dfrac{M}{M_{max}}\right)^{\frac{n}{m}} & n>0 \\ \left(\dfrac{M}{M_{min}}\right)^{\frac{n}{m}} & n<0 \end{cases} \tag{2}$$

The velocity distributions are taken from the Frag Track algorithm. The mass distributions are taken from sieve data of physically captured fragments, from the Frag Track algorithm, and from the use of SigmaScan rear video in the case of the thin glass samples. For size distributions, the masonry and concrete samples created mostly spherical shaped fragments, and the size is determined by a spherical radius. The radius has been calculated by taking the fragment mass data and the known density (measured before testing) and using $m=\rho V$ to calculate the radius. The glass samples fragment into mostly rectangular-shaped fragments. The rectangular shape is defined by a characteristic length that is the longest edge length. The secondary edge length defines the 2nd and 3rd dimension (assumed to be equal) of the rectangular fragment and is captured through an aspect ratio. The edge lengths were taken from SigmaScan analyses of the collected fragments.

## Evidence for a Single Distribution Function Independent of Rate Effects

If the mass, size, or velocity components of distributions are normalized, then the data for varying strain rates collapses on top of each other to form a single distribution. A single function can then be used to describe the shape of these curves. The higher pressure loads create higher velocities and smaller fragments compared to the lower pressure loads, but when the mass, size, and velocity values are normalized the curves fall on top of each other allowing for a single distribution function to describe the fragmentation material behavior. Strain rate is still relevant as the average fragment size and velocity used to normalize the curves vary by strain rate. Figure 10 shows the test data for mass as collected from sieving the physical fragments. The larger load produces a larger number of smaller fragments compared to the smaller load. When the cumulative fragment distributions are normalized by average mass, the data collapses on top of each other suggesting that a single distribution could be used to describe the PDF independent of strain rate.

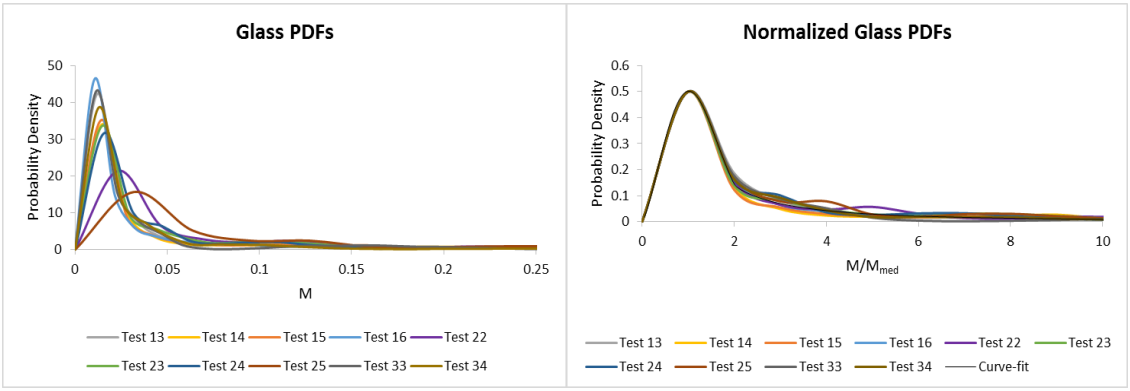


*a* *b*

**Figure 10.** Overlay of glass test mass data a) cumulative fragment distribution and b) normalized by median mass

## Distributions from Sieve Analyses

The fragment data from the sieve analyses were clipped at a minimum size of 0.005-g ($1.1 \times 10^{-5}$-lb). This correlated to the #8 sieve size. The fragments in the #8 sieve size were still large enough that the methodology for measuring the fragments was achievable with a good level of confidence. The fits were determined by calculating the parameters that made the correlation coefficient as close to 1.0 as possible.

For each of the experiments, the histograms were normalized for fragment count on the vertical axis, and then normalized for the median mass on the horizontal axis. The distribution functions were then fit to distributions as illustrated in Figure 11 depicting the normalized glass PDFs with the distribution curve fit overlaid. Figure 12 shows the normalized glass PDFs for size and aspect ratio along with the curve fits. Table 3 shows the summary of the fits and parameters for mass. As might be expected concrete has the largest average fragment size and glass has the smallest average fragment size. Table 5 shows the summary of the fits and parameters for size; rectangular for glass and spherical for concrete and masonry.

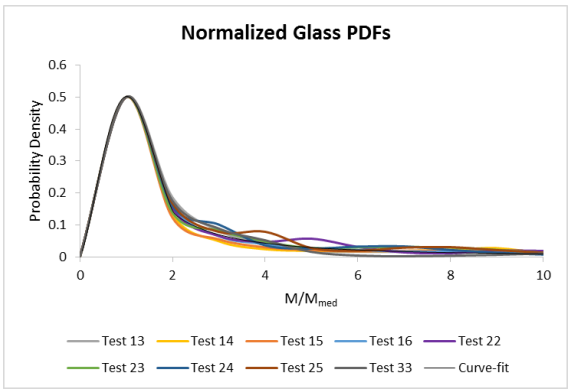


**Figure 11.** Normalized glass PDFs with combined modified Weibull and power law fit

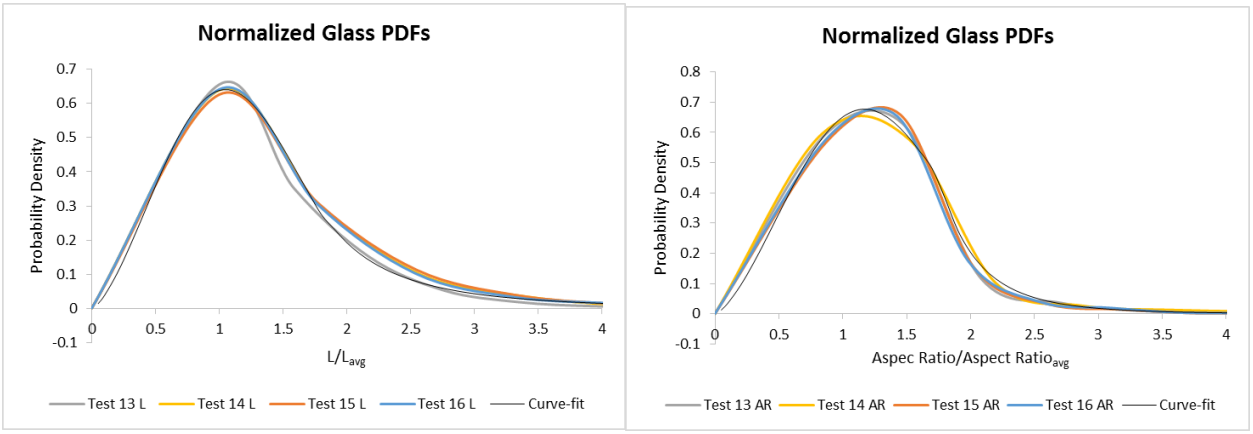


*a* *b*

**Figure 12.** Normalized glass size distribution with combined fit for a) characteristic length and b) aspect ratio

**Table 3.** Summary of distribution parameters for mass sieve analyses

| | Gamma Distribution | | | | Power Distribution | | Mass | |
|---|---|---|---|---|---|---|---|---|
| | α | β | γ | Γ | C | a | Avg. | Std. Dev. |
| Masonry | 1.40E+00 | 2.400 | 1.550 | 1.393 | 0.750 | -2.000 | 0.022 | 0.021 |

| | Gamma Distribution | | | | Power Distribution | | Mass | |
|---|---|---|---|---|---|---|---|---|
| | α | β | γ | Γ | C | a | Avg. | Std. Dev. |
| Glass | 1.30E+00 | 2.300 | 1.420 | 1.451 | 0.450 | -1.700 | 0.013 | 0.012 |

| | Gamma Distribution | | | | Power Distribution | | Mass | |
|---|---|---|---|---|---|---|---|---|
| | α | β | γ | Γ | C | a | Avg. | Std. Dev. |
| Concrete | 1.38E+00 | 2.250 | 1.500 | 1.354 | 0.600 | -1.900 | 0.024 | 0.025 |

**Table 4.** Summary of distribution parameters for size sieve analyses

| | Gamma Distribution | | | | Power Distribution | | Mass | |
|---|---|---|---|---|---|---|---|---|
| | α | β | γ | Γ | C | a | Avg. | Std. Dev. |
| Glass L | 1.30E+00 | 2.450 | 1.900 | 1.193 | 2.500 | -3.700 | 0.371 | 0.274 |

| | Gamma Distribution | | | | Power Distribution | | Mass | |
|---|---|---|---|---|---|---|---|---|
| | α | β | γ | Γ | C | a | Avg. | Std. Dev. |
| Glass AR | 1.45E+00 | 2.450 | 2.400 | 1.012 | 13.000 | -6.000 | 2.358 | 1.437 |

| | Gamma Distribution | | | | Power Distribution | | Mass | |
|---|---|---|---|---|---|---|---|---|
| | α | β | γ | Γ | C | a | Avg. | Std. Dev. |
| Masonry | 1.40E+00 | 2.300 | 2.100 | 1.058 | 4.500 | -4.250 | 0.935 | 0.630 |

| | Gamma Distribution | | | | Power Distribution | | Mass | |
|---|---|---|---|---|---|---|---|---|
| | α | β | γ | Γ | C | a | Avg. | Std. Dev. |
| Concrete | 1.40E+00 | 2.250 | 2.050 | 1.060 | 2.750 | -3.600 | 0.996 | 0.790 |

**Distributions from Frag Track Video Analysis**

The fragment data from the side-view HSV analyses were clipped at a minimum size of 0.5-g (0.0011-lb). As discussed in the Distribution Analysis section, the 0.5-g lower threshold was the minimum size that the video tracking algorithm was able to dependably capture data. Fragment sizes smaller than 0.5-g were tracked, but the level of confidence in the fragment count for the smaller fragments was not good. There is some inconsistency in the data which is most likely due to the fragments that are not being captured during the smoke/fireball obscuration of the tests. As with the sieve test data, the modified Weibull function captures the data the closest. The PDF distributions show a change in slope where there are a sizeable number of larger mass fragments. It is likely that this shows up in the video as larger fragments are easier to capture in the video compared to the smaller fragments. Overall the number of fragments captured by video are less than the number of fragments collected for the sieve analysis (generally on the order of 500 in the video tracking compared to about 4,000 fragments physically collected), so the data could be possibly skewed towards the larger fragments that are better captured by the video analysis than the small fragments. Figure 13 shows the PDFs for glass velocity as well as the normalized version. The normalized version does not overlay as well as the normalized mass and sized PDFs from the sieve analyses, but the trend is still present. Table 5 shows the summary of the parameters and fits for the velocity PDF distributions.

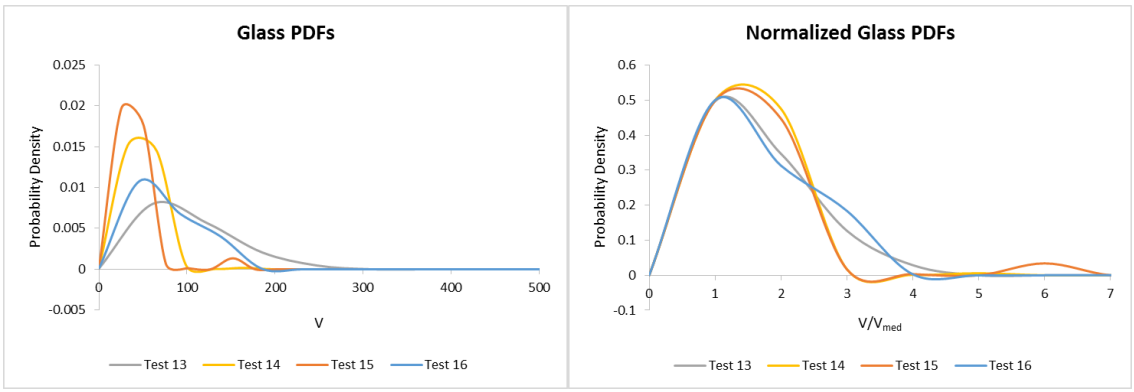


*Test 3* *Test 4*

**Figure 13**. Masonry velocity distribution CDFs for tests 3 and 4

**Table 5.** Summary of distribution parameters for Frag Track velocity analysis

| | Gamma Distribution | | | | Power Distribution | | Mass | |
|---|---|---|---|---|---|---|---|---|
| | α | β | γ | Γ | C | a | Avg. | Std. Dev. |
| Masonry | 1.33E+00 | 2.300 | 1.500 | 1.381 | 0.750 | -2.100 | 98.305 | 60.381 |

| | Gamma Distribution | | | | Power Distribution | | Mass | |
|---|---|---|---|---|---|---|---|---|
| | α | β | γ | Γ | C | a | Avg. | Std. Dev. |
| Glass | 1.30E+00 | 2.300 | 1.420 | 1.451 | 0.450 | -1.700 | 44.900 | 30.105 |

| | Gamma Distribution | | | | Power Distribution | | Mass | |
|---|---|---|---|---|---|---|---|---|
| | α | β | γ | Γ | C | a | Avg. | Std. Dev. |
| Concrete | 1.30E+00 | 2.300 | 1.500 | 1.381 | 0.550 | -1.950 | 92.486 | 68.601 |

## Distributions from SigmaScan Pro Video Analysis

The approach for fitting distributions as described previously was applied to the SigmaScan Pro data for the glass samples. The fragments were assumed to fracture through the entire 6.35-mm (¼") thickness of the glass. As with the sieve data, the fragments were clipped at a minimum fragment size of 0.5-g ($1.1 \times 10^{-5}$-lb). Figure 14 shows the PDF fits for tests 13 and 15. Table 6 shows the corresponding fit parameters.

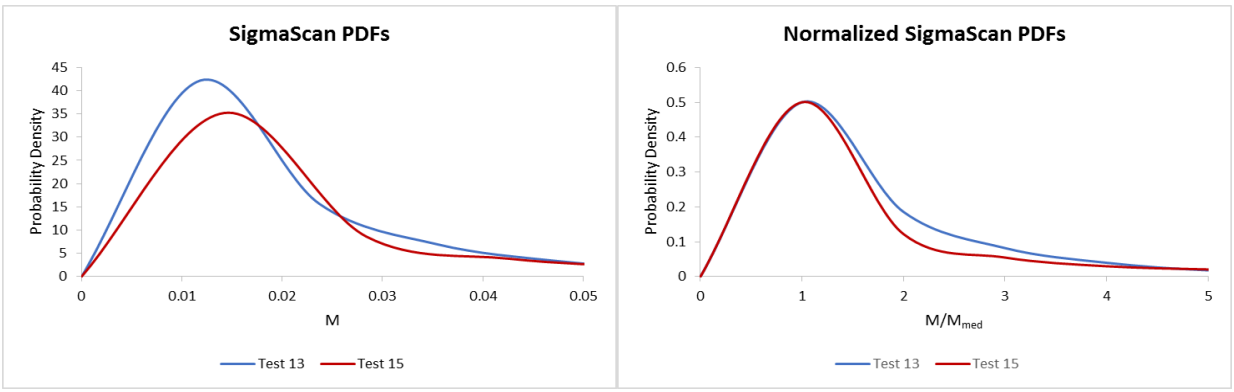


*a)* *b)*

**Figure 14.** Glass SigmaScan developed distribution PDFs for tests 13 and15 for a) regular and b) normalized PDFs

**Table 6.** Function parameters for SigmaScan analysis fits

| | Gamma Distribution | | | | Power Distribution | | Mass | |
|---|---|---|---|---|---|---|---|---|
| | α | β | γ | Γ | C | a | Avg. | Std. Dev. |
| Test 13 | 0.15 | 0.665 | 2.700 | 6.474 | 0.7 | -2.0 | 0.041 | 0.080 |
| Test 15 | 0.10 | 0.650 | 2.700 | 7.303 | 0.3 | -1.5 | 0.087 | 0.182 |

## CONCLUSIONS

Fragment distributions were able to be fit to both mass and velocity using physically collected fragments, the Frag Track algorithm, and SigmaScan techniques. The SigmaScan and physically collected fragments were able to be used and develop good distributions of mass. The Frag Track algorithm was able to produce good information on size and velocity. The modified Weibull combined with the power law function worked quite well, with coefficients of correlation which were above 0.95.

## ACKNOWLEDGMENTS

The authors gratefully acknowledge the financial support provided by the United States of America Defense Threat Reduction Agency, J9 NTES.

## REFERENCES

Barsotti, M., Nelson, L.J., Jones, C., Stevens, D. (2011) Ballistic Glass Hazard Study, Arlington, VA, Technical Support Working Group, Combatting Terrorism Technology Support Office, June 24, 2011.

Stevens, D., Meyer, S., Barsotti, M., Becvar, K., Marchand, K. (2002) *Glass Debris Visualization, Analysis, and Prediction,* Arlington, VA, Technical Support Working Group, Combatting Terrorism Technology Support Office, December, 31, 2002.

# SUPPLEMENTAL INFORMATION

## SUPPLEMENTAL INFORMATION

The supplemental information is mainly a compilation of figures and tables which are not able to fit within the body of the paper. The supplemental information serves the purpose to replace figures in the paper based on review and recommendations from the conference committee who will review the paper. The supplemental information will not be submitted with the original submission of the paper.

### Small Diameter Shock Tube Experiments

Figure 15 through Figure 26 show the pressure history loads that are not included in the main body of the paper.

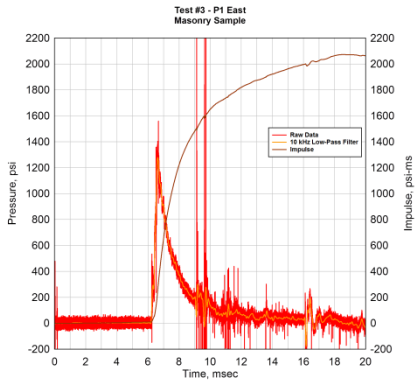


**Figure 15 Test 3 pressure and impulse histories**

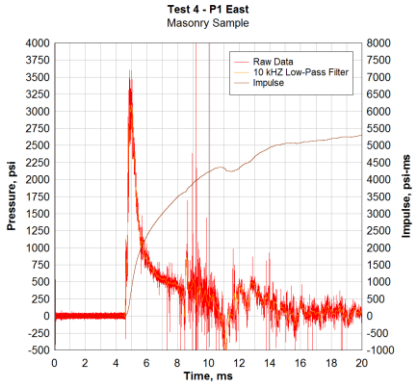


**Figure 16 Test 4 pressure and impulse histories**

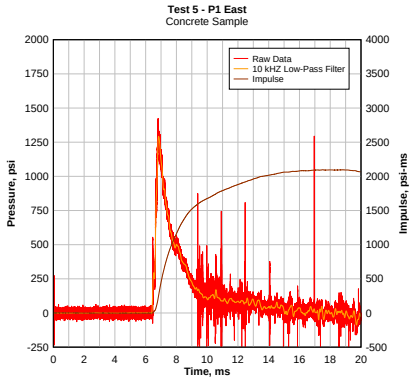


**Figure 17 Test 5 pressure and impulse histories**

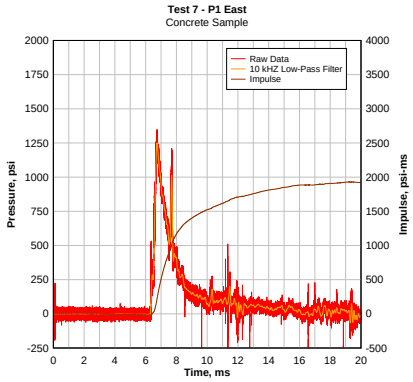


**Figure 18 Test 7 pressure and impulse histories**

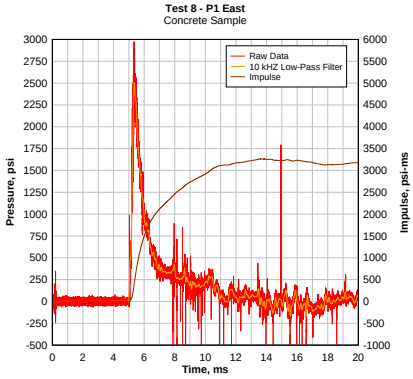


**Figure 19 Test 8 pressure and impulse histories**

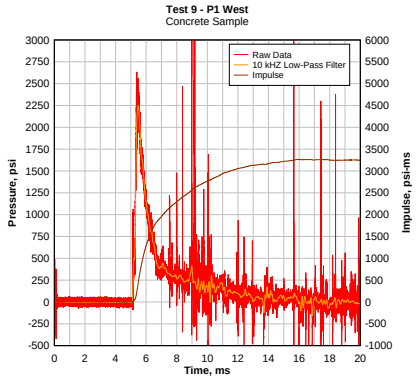


**Figure 20 Test 9 pressure and impulse histories**

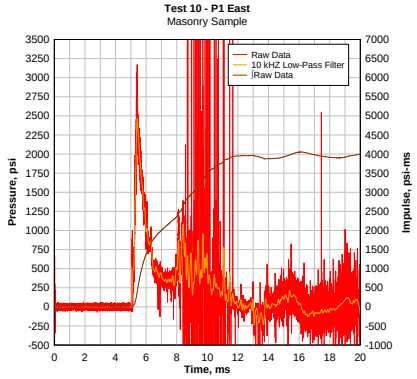


**Figure 21 Test 10 pressure and impulse histories**

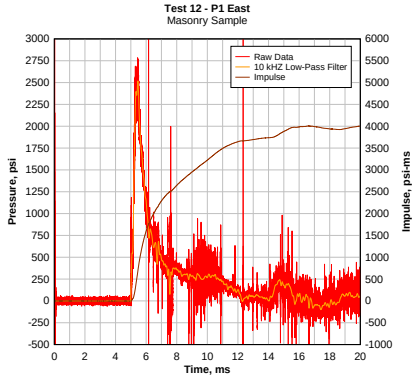


**Figure 22 Test 12 pressure and impulse histories**

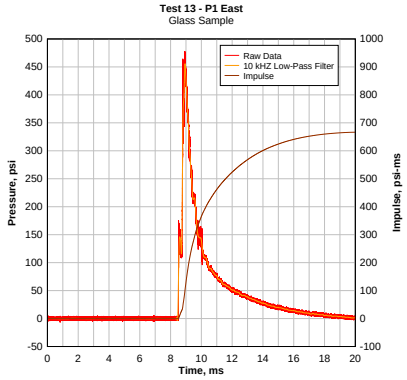


**Figure 23 Test 13 pressure and impulse histories**

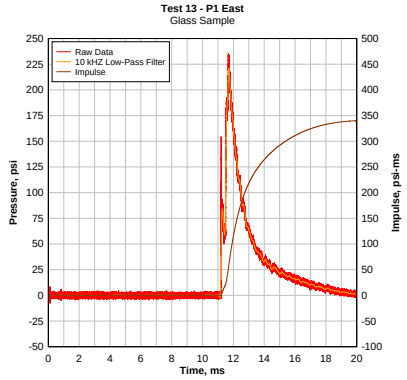


**Figure 24 Test 14 pressure and impulse histories**

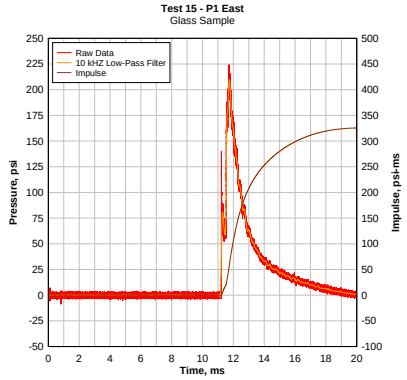


**Figure 25 Test 15 pressure and impulse histories**

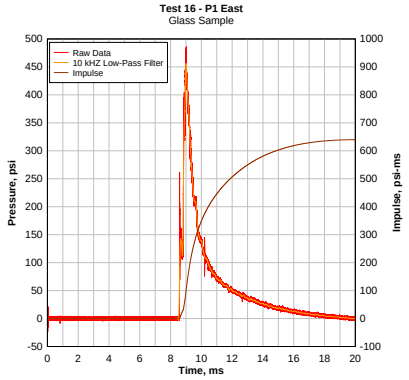


**Figure 26 Test 16 pressure and impulse histories**

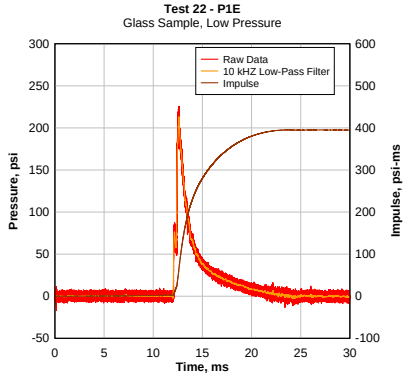


**Figure 27 Test 22 pressure and impulse histories**

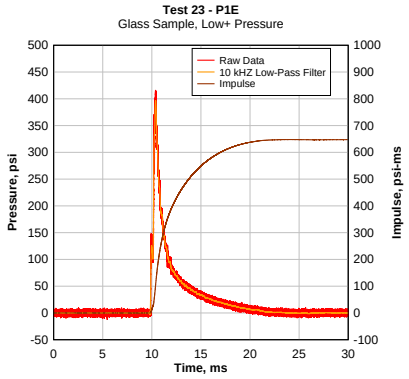


**Figure 28 Test 23 pressure and impulse histories**

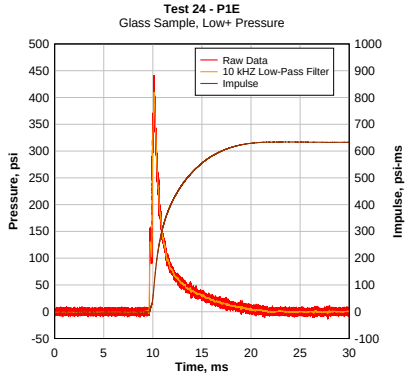


**Figure 29 Test 24 pressure and impulse histories**

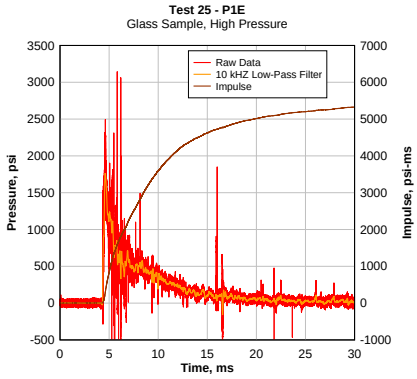


**Figure 30 Test 25 pressure and impulse histories**

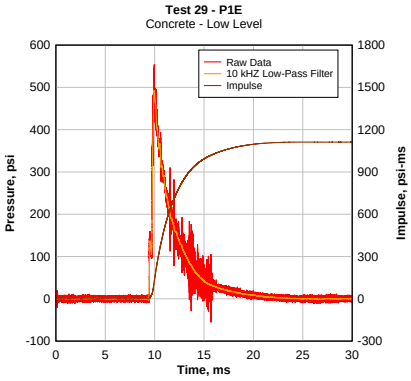


**Figure 31 Test 29 pressure and impulse histories**

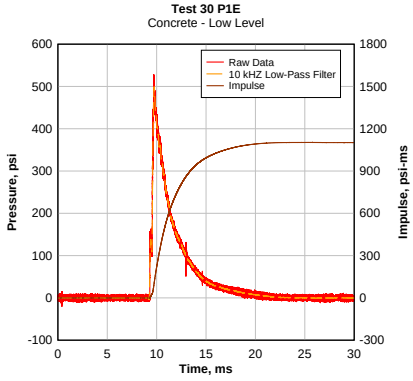


**Figure 32 Test 30 pressure and impulse histories**

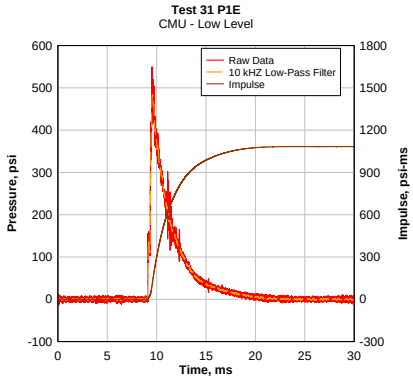


**Figure 33 Test 31 pressure and impulse histories**

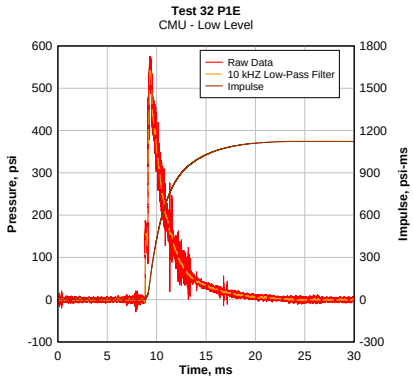


**Figure 34 Test 32 pressure and impulse histories**

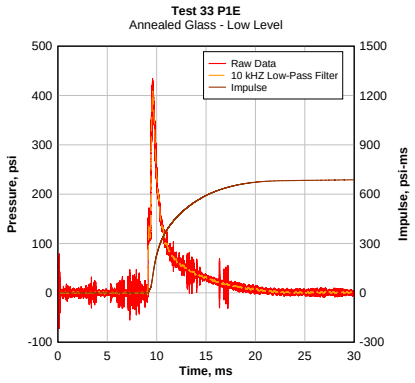


**Figure 35 Test 33 pressure and impulse histories**

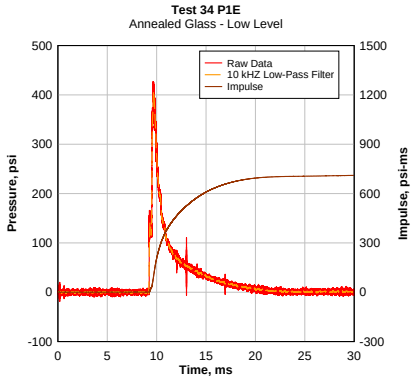


**Figure 36 Test 34 pressure and impulse histories**

## Evidence for a Single Distribution Function Independent of Rate Effects

The single distribution concept is presented in the main body of the paper for the mass, size, and velocity of glass. The following figures show the single distribution concept for concrete and masonry.

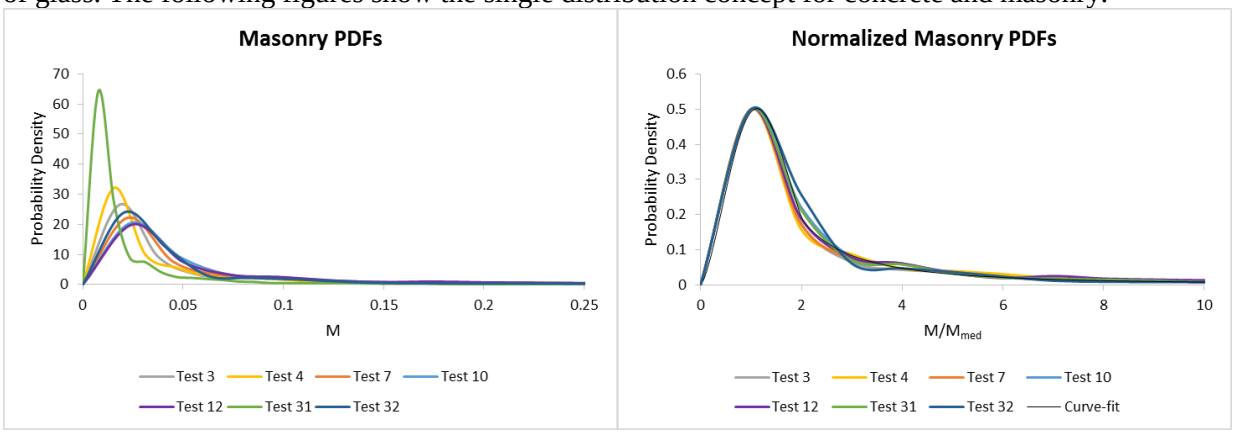


*a* *b*

**Figure 37.** Overlay of masonry test mass data a) PDF and b) normalized by median mass

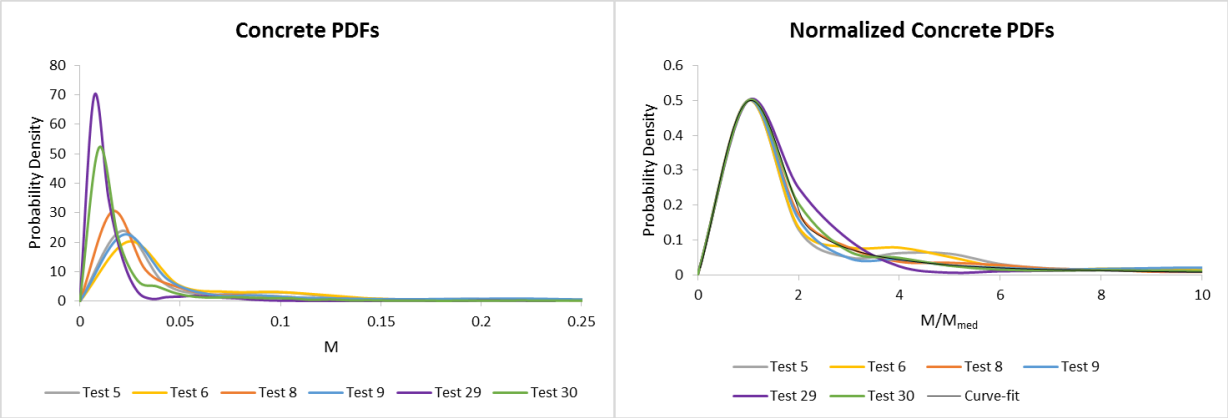


*a* *b*

**Figure 38.** Overlay of concrete test mass data a) PDF and b) normalized by median mass

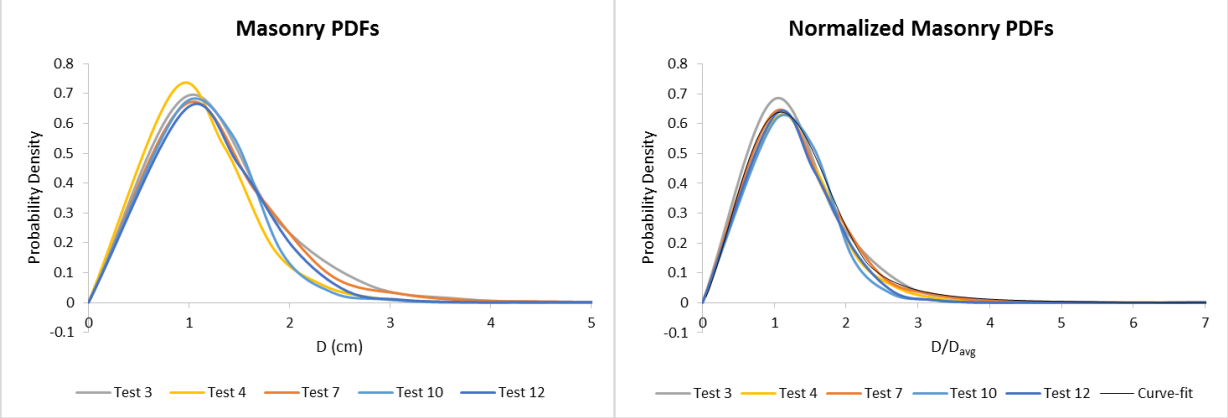


*a* *b*

**Figure 39.** Overlay of masonry test size data a) PDF and b) normalized by median mass

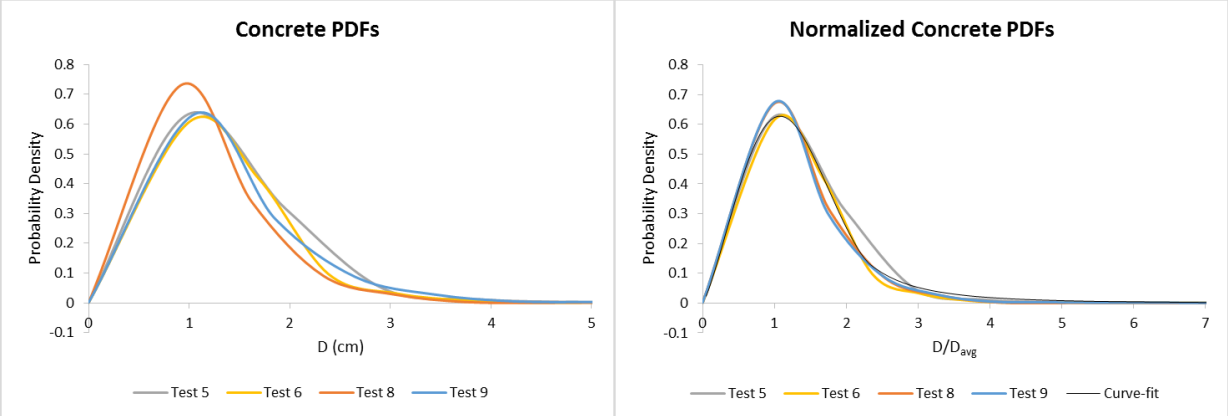


*a* *b*

**Figure 40.** Overlay of concrete test size data a) PDF and b) normalized by median mass

Table 7 through Table 9 list the PDF test data that is grouped by material type. For each experiment there is an average mass, median mass, and the standard deviation with units measured in grams. The tables also list the PDF value by bin number. Bin sizing is incremented by median mass with the first bin covering from 0 to the median mass and each additional bin being incremented by the median mass.

**Table 7** SigmaScan PDF values for masonry tests

| Test No. | 3 | 4 | 7 | 10 | 12 | 31 | 32 |
|---|---|---|---|---|---|---|---|
| Avg. | 0.3675 | 0.0649 | 0.1925 | 0.0957 | 0.0987 | 0.0370 | 0.0633 |
| Med. | 0.0188 | 0.0156 | 0.0225 | 0.0243 | 0.0250 | 0.0078 | 0.0208 |
| Std. Dev. | 5.2564 | 0.3514 | 2.8277 | 1.4648 | 0.8332 | 0.2030 | 0.2940 |
| Bin No. 1 | 0.001 | 0.001 | 0.001 | 0.001 | 0.001 | 0.001 | 0.001 |
| 2 | 26.665 | 32.125 | 22.230 | 20.554 | 19.993 | 64.267 | 24.021 |
| 3 | 9.234 | 10.060 | 7.607 | 9.027 | 7.522 | 27.304 | 12.293 |
| 4 | 3.432 | 5.590 | 3.283 | 3.249 | 3.110 | 8.986 | 2.912 |
| 5 | 2.276 | 2.960 | 2.603 | 2.473 | 2.434 | 7.474 | 2.247 |
| 6 | 1.934 | 2.519 | 1.599 | 1.364 | 1.327 | 4.173 | 1.757 |
| 7 | 1.321 | 1.951 | 0.919 | 0.843 | 0.755 | 2.507 | 1.113 |
| 8 | 0.837 | 1.187 | 0.781 | 0.649 | 0.992 | 2.202 | 0.550 |
| 9 | 0.672 | 0.865 | 0.611 | 0.618 | 0.700 | 1.848 | 0.404 |
| 10 | 0.472 | 0.763 | 0.558 | 0.503 | 0.584 | 1.508 | 0.371 |
| 11 | 0.578 | 0.662 | 0.547 | 0.309 | 0.487 | 0.985 | 0.346 |
| 12 | 0.554 | 0.696 | 0.372 | 0.242 | 0.396 | 0.863 | 0.330 |
| 13 | 0.472 | 0.517 | 0.351 | 0.188 | 0.250 | 0.518 | 0.269 |
| 14 | 0.366 | 0.492 | 0.250 | 0.103 | 0.146 | 0.454 | 0.182 |
| 15 | 0.318 | 0.407 | 0.202 | 0.121 | 0.122 | 0.386 | 0.140 |
| 16 | 0.271 | 0.382 | 0.133 | 0.067 | 0.103 | 0.418 | 0.100 |
| 17 | 0.200 | 0.263 | 0.143 | 0.067 | 0.067 | 0.404 | 0.071 |
| 18 | 0.165 | 0.187 | 0.112 | 0.079 | 0.097 | 0.445 | 0.042 |
| 19 | 0.165 | 0.187 | 0.106 | 0.055 | 0.073 | 0.354 | 0.038 |
| 20 | 0.165 | 0.195 | 0.096 | 0.030 | 0.049 | 0.295 | 0.035 |
| 21 | 0.212 | 0.178 | 0.085 | 0.042 | 0.049 | 0.250 | 0.040 |
| 22 | 0.153 | 0.093 | 0.090 | 0.036 | 0.049 | 0.245 | 0.036 |
| 23 | 0.035 | 0.187 | 0.101 | 0.036 | 0.061 | 0.259 | 0.044 |
| 24 | 0.106 | 0.136 | 0.112 | 0.036 | 0.049 | 0.150 | 0.055 |
| 25 | 0.177 | 0.127 | 0.074 | 0.030 | 0.055 | 0.168 | 0.046 |
| 26 | 0.189 | 0.059 | 0.032 | 0.036 | 0.030 | 0.123 | 0.049 |
| 27 | 0.177 | 0.085 | 0.074 | 0.036 | 0.030 | 0.045 | 0.033 |
| 28 | 0.083 | 0.102 | 0.080 | 0.012 | 0.049 | 0.054 | 0.025 |
| 29 | 0.083 | 0.085 | 0.037 | 0.018 | 0.049 | 0.050 | 0.040 |
| 30 | 0.106 | 0.068 | 0.042 | 0.006 | 0.024 | 0.018 | 0.020 |
| 31 | 0.035 | 0.068 | 0.106 | 0.024 | 0.006 | 0.014 | 0.029 |
| 32 | 0.059 | 0.093 | 0.058 | 0.018 | 0.024 | 0.000 | 0.013 |
| 33 | 0.083 | 0.017 | 0.032 | 0.018 | 0.012 | 0.005 | 0.031 |
| 34 | 0.071 | 0.068 | 0.058 | 0.018 | 0.006 | 0.005 | 0.015 |

**Table 8.** SigmaScan PDF values for concrete tests

| Test No. | 5 | 6 | 8 | 9 | 29 | 30 |
|---|---|---|---|---|---|---|
| Avg. | 0.4732 | 0.1808 | 0.2246 | 0.2482 | 0.0349 | 0.0564 |
| Med. | 0.0209 | 0.0246 | 0.0164 | 0.0221 | 0.0072 | 0.0096 |
| Std. Dev. | 9.0826 | 2.9202 | 3.8470 | 3.3618 | 0.1414 | 0.2258 |
| Bin No. 1 | 0.001 | 0.001 | 0.001 | 0.001 | 0.001 | 0.001 |
| 2 | 23.892 | 20.332 | 22.664 | 22.664 | 69.713 | 52.120 |
| 3 | 6.220 | 5.539 | 7.250 | 7.250 | 34.798 | 21.316 |
| 4 | 2.383 | 3.198 | 2.165 | 2.165 | 13.991 | 7.044 |
| 5 | 2.976 | 3.165 | 2.016 | 2.016 | 3.376 | 5.065 |
| 6 | 2.887 | 2.081 | 1.212 | 1.212 | 0.813 | 2.709 |
| 7 | 1.473 | 0.878 | 0.904 | 0.904 | 1.410 | 1.518 |
| 8 | 0.860 | 0.542 | 0.675 | 0.675 | 1.598 | 1.275 |
| 9 | 0.702 | 0.705 | 0.755 | 0.755 | 1.897 | 1.400 |
| 10 | 0.752 | 0.672 | 0.854 | 0.854 | 1.521 | 1.191 |
| 11 | 0.722 | 0.531 | 0.934 | 0.934 | 1.209 | 1.031 |
| 12 | 0.574 | 0.314 | 0.695 | 0.695 | 0.980 | 0.989 |
| 13 | 0.405 | 0.336 | 0.536 | 0.536 | 0.556 | 0.470 |
| 14 | 0.277 | 0.163 | 0.387 | 0.387 | 0.333 | 0.621 |
| 15 | 0.237 | 0.119 | 0.288 | 0.288 | 0.201 | 0.310 |
| 16 | 0.218 | 0.087 | 0.238 | 0.238 | 0.174 | 0.327 |
| 17 | 0.109 | 0.087 | 0.109 | 0.109 | 0.097 | 0.226 |
| 18 | 0.119 | 0.043 | 0.129 | 0.129 | 0.069 | 0.210 |
| 19 | 0.079 | 0.076 | 0.119 | 0.119 | 0.118 | 0.193 |
| 20 | 0.069 | 0.087 | 0.149 | 0.149 | 0.104 | 0.159 |
| 21 | 0.059 | 0.065 | 0.119 | 0.119 | 0.125 | 0.201 |
| 22 | 0.099 | 0.119 | 0.139 | 0.139 | 0.174 | 0.252 |
| 23 | 0.069 | 0.098 | 0.139 | 0.139 | 0.208 | 0.210 |
| 24 | 0.099 | 0.108 | 0.149 | 0.149 | 0.236 | 0.260 |
| 25 | 0.099 | 0.043 | 0.189 | 0.189 | 0.174 | 0.184 |
| 26 | 0.119 | 0.087 | 0.099 | 0.099 | 0.160 | 0.226 |
| 27 | 0.109 | 0.054 | 0.099 | 0.099 | 0.153 | 0.201 |
| 28 | 0.089 | 0.033 | 0.129 | 0.129 | 0.174 | 0.218 |
| 29 | 0.109 | 0.043 | 0.119 | 0.119 | 0.292 | 0.092 |
| 30 | 0.069 | 0.054 | 0.099 | 0.099 | 0.264 | 0.176 |
| 31 | 0.040 | 0.043 | 0.109 | 0.109 | 0.167 | 0.193 |
| 32 | 0.099 | 0.065 | 0.040 | 0.040 | 0.181 | 0.134 |
| 33 | 0.069 | 0.022 | 0.089 | 0.089 | 0.125 | 0.134 |
| 34 | 0.049 | 0.108 | 0.060 | 0.060 | 0.090 | 0.075 |

**Table 9.** SigmaScan PDF values for glass tests

| Test No. | 13 | 14 | 15 | 16 | 22 | 23 | 24 | 25 | 33 | 34 |
|---|---|---|---|---|---|---|---|---|---|---|
| Avg. | 0.0411 | 0.0827 | 0.0866 | 0.0513 | 0.0721 | 0.0479 | 0.0457 | 0.0783 | 0.0713 | 0.0915 |
| Med. | 0.0119 | 0.0147 | 0.0142 | 0.0108 | 0.0233 | 0.0149 | 0.0158 | 0.0319 | 0.0116 | 0.0129 |
| Std. Dev. | 0.0797 | 0.1708 | 0.1820 | 0.1253 | 0.1202 | 0.0731 | 0.0727 | 0.1219 | 0.2898 | 0.3411 |
| Bin No. 1 | 0.0001 | 0.0001 | 0.0001 | 0.0001 | 0.001 | 0.001 | 0.001 | 0.001 | 0.001 | 0.001 |
| 2 | 42.207 | 34.068 | 35.207 | 46.443 | 21.432 | 33.684 | 31.671 | 15.692 | 43.127 | 38.652 |
| 3 | 15.674 | 9.025 | 8.594 | 14.931 | 6.465 | 9.269 | 10.027 | 5.235 | 15.077 | 12.502 |
| 4 | 6.912 | 3.332 | 3.855 | 6.023 | 2.800 | 5.546 | 6.391 | 2.454 | 7.631 | 7.096 |
| 5 | 3.360 | 1.618 | 2.104 | 3.739 | 2.023 | 3.209 | 2.281 | 2.463 | 4.469 | 3.380 |
| 6 | 1.531 | 1.276 | 1.455 | 2.484 | 2.436 | 1.835 | 1.634 | 0.865 | 1.331 | 1.374 |
| 7 | 1.297 | 1.238 | 1.200 | 2.008 | 1.323 | 1.988 | 2.020 | 0.597 | 0.340 | 1.439 |
| 8 | 1.297 | 1.257 | 1.357 | 1.556 | 0.591 | 2.087 | 2.066 | 0.902 | 0.149 | 1.393 |
| 9 | 1.510 | 1.504 | 1.337 | 1.506 | 0.481 | 1.956 | 1.358 | 0.949 | 0.303 | 1.284 |
| 10 | 1.829 | 1.847 | 1.200 | 1.405 | 0.842 | 1.496 | 0.820 | 0.666 | 0.538 | 0.929 |
| 11 | 0.978 | 0.914 | 1.042 | 0.778 | 0.794 | 0.889 | 0.456 | 0.417 | 0.885 | 0.652 |
| 12 | 0.957 | 1.009 | 1.259 | 0.878 | 0.859 | 0.655 | 0.541 | 0.253 | 1.108 | 0.406 |
| 13 | 0.404 | 0.743 | 0.865 | 0.828 | 0.656 | 0.476 | 0.608 | 0.125 | 1.052 | 0.271 |
| 14 | 0.447 | 0.819 | 0.708 | 0.878 | 0.437 | 0.572 | 0.674 | 0.110 | 1.157 | 0.194 |
| 15 | 0.276 | 0.800 | 0.728 | 0.728 | 0.354 | 0.547 | 0.525 | 0.110 | 1.201 | 0.148 |
| 16 | 0.489 | 0.724 | 0.669 | 0.527 | 0.227 | 0.499 | 0.443 | 0.054 | 1.009 | 0.252 |
| 17 | 0.532 | 0.628 | 0.669 | 0.627 | 0.127 | 0.435 | 0.431 | 0.061 | 0.817 | 0.232 |
| 18 | 0.468 | 0.762 | 0.669 | 0.602 | 0.133 | 0.355 | 0.307 | 0.048 | 0.774 | 0.245 |
| 19 | 0.510 | 0.838 | 0.708 | 0.326 | 0.106 | 0.352 | 0.216 | 0.032 | 0.569 | 0.335 |
| 20 | 0.447 | 0.590 | 0.295 | 0.602 | 0.083 | 0.300 | 0.164 | 0.035 | 0.489 | 0.310 |
| 21 | 0.362 | 0.666 | 0.433 | 0.402 | 0.047 | 0.185 | 0.131 | 0.039 | 0.359 | 0.348 |
| 22 | 0.319 | 0.343 | 0.275 | 0.351 | 0.047 | 0.150 | 0.112 | 0.035 | 0.229 | 0.264 |
| 23 | 0.234 | 0.267 | 0.354 | 0.301 | 0.059 | 0.105 | 0.082 | 0.035 | 0.217 | 0.232 |
| 24 | 0.340 | 0.267 | 0.433 | 0.427 | 0.032 | 0.118 | 0.043 | 0.043 | 0.136 | 0.219 |
| 25 | 0.255 | 0.400 | 0.275 | 0.376 | 0.038 | 0.089 | 0.046 | 0.028 | 0.111 | 0.316 |
| 26 | 0.276 | 0.152 | 0.216 | 0.326 | 0.027 | 0.054 | 0.018 | 0.017 | 0.093 | 0.200 |
| 27 | 0.170 | 0.076 | 0.315 | 0.326 | 0.032 | 0.048 | 0.027 | 0.017 | 0.043 | 0.239 |
| 28 | 0.106 | 0.171 | 0.118 | 0.226 | 0.038 | 0.051 | 0.018 | 0.013 | 0.062 | 0.174 |
| 29 | 0.170 | 0.248 | 0.177 | 0.326 | 0.035 | 0.038 | 0.015 | 0.013 | 0.043 | 0.142 |
| 30 | 0.064 | 0.076 | 0.236 | 0.176 | 0.035 | 0.054 | 0.015 | 0.015 | 0.043 | 0.142 |
| 31 | 0.106 | 0.076 | 0.098 | 0.276 | 0.030 | 0.016 | 0.012 | 0.002 | 0.025 | 0.103 |
| 32 | 0.043 | 0.171 | 0.236 | 0.151 | 0.024 | 0.022 | 0.006 | 0.006 | 0.031 | 0.071 |
| 33 | 0.043 | 0.152 | 0.157 | 0.176 | 0.047 | 0.029 | 0.009 | 0.006 | 0.025 | 0.090 |
| 34 | 0.021 | 0.076 | 0.197 | 0.125 | 0.027 | 0.035 | 0.006 | 0.002 | 0.012 | 0.058 |

Table 10 through
Table 12Table 9 lists PDF test data that is grouped by material type. Data for these tables is based on size in centimeters, and similar to Table 7 through Table 9 each table contains an average size, median size, and standard deviation for each experiment. The tables list the PDF value by bin number, where bin sizing is also incremented by the individual median. The first bin covers from 0 to the median size value and each bin is then incremented by the median size value. Table 10 and 11 show the radius assuming a spherical fragment. Table 12 shows the characteristic length and the corresponding aspect ratio based on a rectangular fragment.

**Table 10.** SigmaScan PDF values for masonry tests

| Test No. | 3 | 4 | 7 | 10 | 12 | 31 | 32 |
|---|---|---|---|---|---|---|---|
| Avg. | 0.9848 | 0.8580 | 0.9615 | 0.9240 | 0.9672 | 0.6891 | 0.9259 |
| Med. | 0.7670 | 0.7209 | 0.8149 | 0.8365 | 0.8440 | 0.5719 | 0.7938 |
| Std. Dev. | 0.8996 | 0.4915 | 0.7202 | 0.5015 | 0.5368 | 0.3902 | 0.4048 |
| Bin No. 1 | 0.00100 | 0.00100 | 0.00100 | 0.00100 | 0.00100 | 0.00100 | 0.00100 |
| 2 | 0.65186 | 0.69359 | 0.61347 | 0.59765 | 0.59173 | 0.87257 | 0.62898 |
| 3 | 0.48197 | 0.54295 | 0.48045 | 0.53010 | 0.49857 | 0.74082 | 0.55733 |
| 4 | 0.11883 | 0.12351 | 0.09709 | 0.05908 | 0.08126 | 0.10772 | 0.05901 |
| 5 | 0.03317 | 0.02162 | 0.02449 | 0.00564 | 0.00919 | 0.00241 | 0.01021 |
| 6 | 0.00750 | 0.00312 | 0.00499 | 0.00071 | 0.00072 | 0.01426 | 0.00119 |
| 7 | 0.00115 | 0.00037 | 0.00293 | 0.00071 | 0.00162 | 0.00580 | 0.00124 |
| 8 | 0.00029 | 0.00037 | 0.00044 | 0.00035 | 0.00018 | 0.00259 | 0.00124 |
| 9 | 0.00087 | 0.00128 | 0.00073 | 0.00053 | 0.00054 | 0.00154 | 0.00052 |
| 10 | 0.00115 | 0.00018 | 0.00029 | 0.00000 | 0.00072 | 0.00062 | 0.00000 |
| 11 | 0.00115 | 0.00000 | 0.00044 | 0.00000 | 0.00000 | 0.00031 | 0.00000 |
| 12 | 0.00144 | 0.00018 | 0.00029 | 0.00035 | 0.00018 | 0.00000 | 0.00000 |
| 13 | 0.00087 | 0.00000 | 0.00000 | 0.00000 | 0.00000 | 0.00000 | 0.00000 |
| 14 | 0.00115 | 0.00000 | 0.00000 | 0.00000 | 0.00018 | 0.00000 | 0.00000 |
| 15 | 0.00029 | 0.00000 | 0.00000 | 0.00000 | 0.00000 | 0.00000 | 0.00000 |
| 16 | 0.00029 | 0.00000 | 0.00000 | 0.00018 | 0.00000 | 0.00000 | 0.00000 |
| 17 | 0.00058 | 0.00000 | 0.00000 | 0.00018 | 0.00000 | 0.00000 | 0.00000 |
| 18 | 0.00029 | 0.00000 | 0.00000 | 0.00000 | 0.00000 | 0.00000 | 0.00000 |
| 19 | 0.00000 | 0.00000 | 0.00000 | 0.00000 | 0.00000 | 0.00000 | 0.00000 |
| 20 | 0.00029 | 0.00000 | 0.00000 | 0.00000 | 0.00000 | 0.00000 | 0.00000 |

**Table 11.** SigmaScan PDF values for concrete tests

| Test No. | 5 | 6 | 8 | 9 | 29 | 30 |
|---|---|---|---|---|---|---|
| Avg. | 0.9895 | 1.0093 | 0.9173 | 1.0611 | 0.6190 | 0.7782 |
| Med. | 0.7939 | 0.8378 | 0.7316 | 0.8080 | 0.5555 | 0.6121 |
| Std. Dev. | 0.9693 | 0.6866 | 0.7084 | 0.7967 | 0.4426 | 0.4795 |
| Bin No. 1 | 0.00100 | 0.00100 | 0.00100 | 0.00100 | 0.00010 | 0.00010 |
| 2 | 0.62964 | 0.59666 | 0.61857 | 0.61857 | 0.89851 | 0.81586 |
| 3 | 0.46147 | 0.47287 | 0.40894 | 0.40894 | 0.74705 | 0.63189 |
| 4 | 0.11341 | 0.09165 | 0.15023 | 0.15023 | 0.08733 | 0.11721 |
| 5 | 0.03728 | 0.02355 | 0.04447 | 0.04447 | 0.03255 | 0.03653 |
| 6 | 0.00652 | 0.00318 | 0.00542 | 0.00542 | 0.02277 | 0.02286 |
| 7 | 0.00391 | 0.00159 | 0.00298 | 0.00298 | 0.00879 | 0.00618 |
| 8 | 0.00156 | 0.00159 | 0.00190 | 0.00190 | 0.00287 | 0.00105 |
| 9 | 0.00052 | 0.00064 | 0.00190 | 0.00190 | 0.00036 | 0.00197 |
| 10 | 0.00052 | 0.00064 | 0.00054 | 0.00054 | 0.00000 | 0.00026 |
| 11 | 0.00052 | 0.00032 | 0.00081 | 0.00081 | 0.00000 | 0.00000 |
| 12 | 0.00052 | 0.00032 | 0.00081 | 0.00081 | 0.00000 | 0.00000 |
| 13 | 0.00052 | 0.00032 | 0.00054 | 0.00054 | 0.00000 | 0.00000 |
| 14 | 0.00078 | 0.00000 | 0.00000 | 0.00000 | 0.00000 | 0.00000 |
| 15 | 0.00026 | 0.00000 | 0.00000 | 0.00000 | 0.00000 | 0.00000 |
| 16 | 0.00052 | 0.00000 | 0.00000 | 0.00000 | 0.00000 | 0.00000 |
| 17 | 0.00000 | 0.00000 | 0.00000 | 0.00000 | 0.00000 | 0.00000 |
| 18 | 0.00026 | 0.00000 | 0.00000 | 0.00000 | 0.00000 | 0.00000 |
| 19 | 0.00000 | 0.00000 | 0.00000 | 0.00000 | 0.00000 | 0.00000 |
| 20 | 0.00052 | 0.00000 | 0.00027 | 0.00027 | 0.00000 | 0.00000 |

**Table 12.** SigmaScan PDF values for glass tests

| Test No. | 13 L[1] | 13 AR[1] | 14 L | 14 AR | 15 L | 15 AR | 16 L | 16 AR |
|---|---|---|---|---|---|---|---|---|
| Avg. | 0.3283 | 2.2457 | 0.4111 | 2.5753 | 0.4010 | 2.3699 | 0.3498 | 2.3951 |
| Med. | 0.2618 | 1.8869 | 0.2973 | 2.0690 | 0.2964 | 2.0703 | 0.2633 | 2.0767 |
| Std. Dev. | 0.1926 | 1.7192 | 0.3234 | 2.8679 | 0.3108 | 1.4266 | 0.2687 | 1.3379 |
| Bin No. 1 | 0.00010 | 0.00010 | 0.00010 | 0.00010 | 0.00010 | 0.00010 | 0.00010 | 0.00010 |
| 2 | 1.90940 | 0.26492 | 1.68168 | 0.24166 | 1.68723 | 0.24151 | 1.89826 | 0.24071 |
| 3 | 1.39202 | 0.28373 | 0.97609 | 0.23393 | 0.97569 | 0.27851 | 1.19675 | 0.27311 |
| 4 | 0.38437 | 0.05189 | 0.44342 | 0.04096 | 0.45765 | 0.06403 | 0.46455 | 0.07226 |
| 5 | 0.10019 | 0.01638 | 0.16722 | 0.01066 | 0.15947 | 0.01355 | 0.13126 | 0.01635 |
| 6 | 0.02119 | 0.00442 | 0.04791 | 0.00516 | 0.05662 | 0.00616 | 0.05948 | 0.00807 |
| 7 | 0.00963 | 0.00276 | 0.02349 | 0.00283 | 0.02359 | 0.00082 | 0.02769 | 0.00141 |
| 8 | 0.00193 | 0.00184 | 0.01127 | 0.00067 | 0.00755 | 0.00103 | 0.01025 | 0.00121 |
| 9 | 0.00096 | 0.00074 | 0.00564 | 0.00100 | 0.00472 | 0.00103 | 0.00513 | 0.00020 |
| 10 | 0.00000 | 0.00110 | 0.00282 | 0.00000 | 0.00094 | 0.00041 | 0.00205 | 0.00020 |
| 11 | 0.00000 | 0.00055 | 0.00282 | 0.00017 | 0.00094 | 0.00021 | 0.00000 | 0.00000 |
| 12 | 0.00000 | 0.00018 | 0.00094 | 0.00017 | 0.00000 | 0.00000 | 0.00000 | 0.00000 |
| 13 | 0.00000 | 0.00000 | 0.00000 | 0.00000 | 0.00000 | 0.00000 | 0.00103 | 0.00000 |
| 14 | 0.00000 | 0.00000 | 0.00000 | 0.00000 | 0.00000 | 0.00021 | 0.00103 | 0.00020 |
| 15 | 0.00000 | 0.00000 | 0.00000 | 0.00000 | 0.00000 | 0.00000 | 0.00000 | 0.00000 |
| 16 | 0.00000 | 0.00018 | 0.00000 | 0.00117 | 0.00000 | 0.00000 | 0.00000 | 0.00000 |
| 17 | 0.00000 | 0.00018 | 0.00000 | 0.00000 | 0.00000 | 0.00000 | 0.00000 | 0.00000 |
| 18 | 0.00000 | 0.00000 | 0.00000 | 0.00000 | 0.00000 | 0.00000 | 0.00000 | 0.00000 |
| 19 | 0.00000 | 0.00055 | 0.00000 | 0.00000 | 0.00000 | 0.00082 | 0.00000 | 0.00081 |
| 20 | 0.00000 | 0.00000 | 0.00000 | 0.00000 | 0.00000 | 0.00000 | 0.00000 | 0.00000 |

*Notes: 1. L – Length; AR – Aspect Ratio*

## Distributions from Sieve Analyses

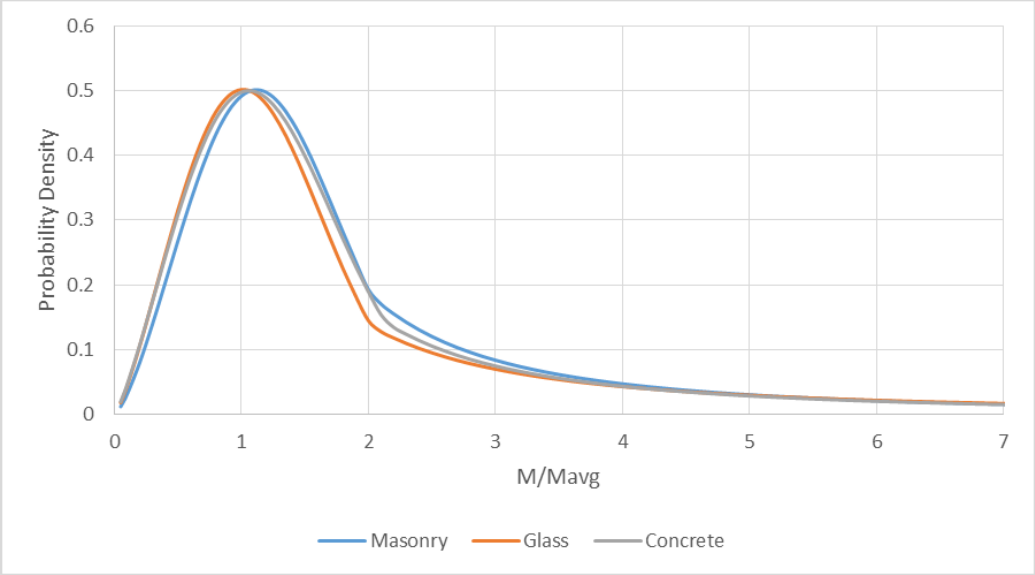


**Figure 41 Overlay of average modified Weibull distribution fits**

**Table 13.** Masonry function parameters for SigmaScan analysis fits

| Masonry | Gamma Distribution | | | | Power Distribution | | Mass | |
|---|---|---|---|---|---|---|---|---|
| Test No. | α | β | γ | Γ | C | a | Avg. | Std. Dev. |
| 3 | 0.40 | 0.850 | 2.050 | 1.252 | 0.5 | -1.8 | 0.367 | 5.256 |
| 4 | 0.25 | 0.750 | 2.250 | 2.000 | 0.4 | -1.6 | 0.065 | 0.351 |
| 7 | 0.40 | 0.850 | 2.050 | 1.252 | 0.5 | -1.6 | 0.193 | 2.828 |
| 10 | 0.52 | 0.900 | 2.050 | 1.151 | 0.8 | -2.0 | 0.096 | 1.465 |
| 12 | 0.50 | 0.910 | 2.050 | 1.135 | 0.6 | -1.7 | 0.099 | 0.833 |
| 31 | 0.45 | 0.870 | 2.200 | 1.357 | 0.7 | -2.0 | 0.037 | 0.203 |
| 32 | 0.61 | 0.960 | 2.050 | 1.065 | 0.7 | -2.0 | 0.063 | 0.294 |

**Table 14.** Concrete function parameters for SigmaScan analysis fits

| Concrete | Gamma Distribution | | | | Power Distribution | | Mass | |
|---|---|---|---|---|---|---|---|---|
| Test No. | α | β | γ | Γ | C | a | Avg. | Std. Dev. |
| 5 | 0.25 | 0.775 | 2.200 | 1.732 | 0.3 | -1.5 | 0.473 | 9.083 |
| 6 | 0.27 | 0.775 | 2.150 | 1.641 | 0.4 | -1.7 | 0.181 | 2.920 |
| 8 | 0.30 | 0.775 | 2.200 | 1.732 | 0.6 | -1.9 | 0.225 | 3.847 |
| 9 | 0.28 | 0.775 | 2.200 | 1.732 | 0.3 | -1.5 | 0.248 | 3.362 |
| 29 | 0.45 | 0.860 | 2.300 | 1.514 | 0.3 | -1.5 | 0.035 | 0.141 |
| 30 | 0.28 | 0.750 | 2.300 | 2.129 | 0.3 | -1.5 | 0.056 | 0.226 |

**Table 15.** Glass function parameters for SigmaScan analysis fits

| Glass | Gamma Distribution | | | | Power Distribution | | Mass | |
|---|---|---|---|---|---|---|---|---|
| Test No. | α | β | γ | Γ | C | a | Avg. | Std. Dev. |
| 13 | 0.15 | 0.665 | 2.700 | 6.474 | 0.7 | -2.0 | 0.041 | 0.080 |
| 14 | 0.10 | 0.650 | 2.700 | 7.303 | 0.3 | -1.5 | 0.083 | 0.171 |
| 15 | 0.10 | 0.650 | 2.700 | 7.303 | 0.3 | -1.5 | 0.087 | 0.182 |
| 16 | 0.10 | 0.620 | 2.700 | 9.533 | 0.5 | -1.7 | 0.051 | 0.125 |
| 22 | 0.38 | 0.850 | 2.050 | 1.252 | 0.5 | -1.7 | 0.072 | 0.120 |
| 23 | 0.27 | 0.775 | 2.150 | 1.641 | 0.5 | -1.7 | 0.048 | 0.073 |
| 24 | 0.30 | 0.775 | 2.200 | 1.732 | 0.5 | -1.7 | 0.046 | 0.073 |
| 25 | 0.38 | 0.850 | 2.050 | 1.252 | 0.6 | -2.0 | 0.078 | 0.122 |
| 33 | 0.19 | 0.700 | 2.350 | 2.849 | 0.7 | -2.0 | 0.071 | 0.290 |
| 34 | 0.19 | 0.700 | 2.350 | 2.849 | 0.5 | -1.7 | 0.092 | 0.341 |

### Distributions from Frag Track Video Analysis

The data from the Frag Track algorithm has also been used to develop velocity distributions. For several of the cases the mid-range velocities were obscured out by smoke and fire. Figure 42 shows the smoke obscuration that occurs and then the subsequent fragments that are picked up at late time with slower velocities. This issue occurs on some of the tests, but not all. Due to these issues, the probability distribution functions are not as smooth as the mass data.

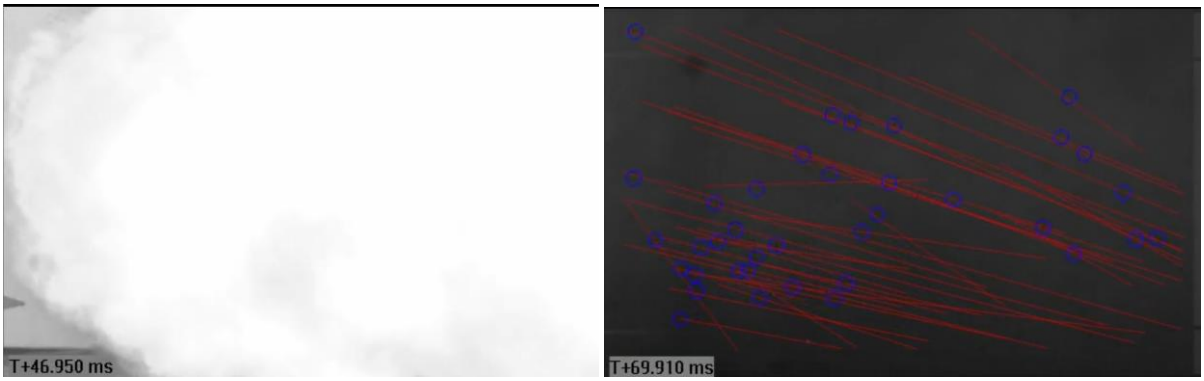


**Figure 42 Test 4 video at 47-msec and 69-msec – illustration of smoke obscuration of velocity measurements**

Because the histogram data had a fair amount of scatter, the same approach that was applied to the mass data was applied to the velocity data in order to reduce the numerical noise from the data scatter. The data was placed into normalized PDFs and functions were fit to the data. As with the mass data, the modified Weibull function and power law were the best fitting. The figures below show the PDF and the normalized version of the PDF

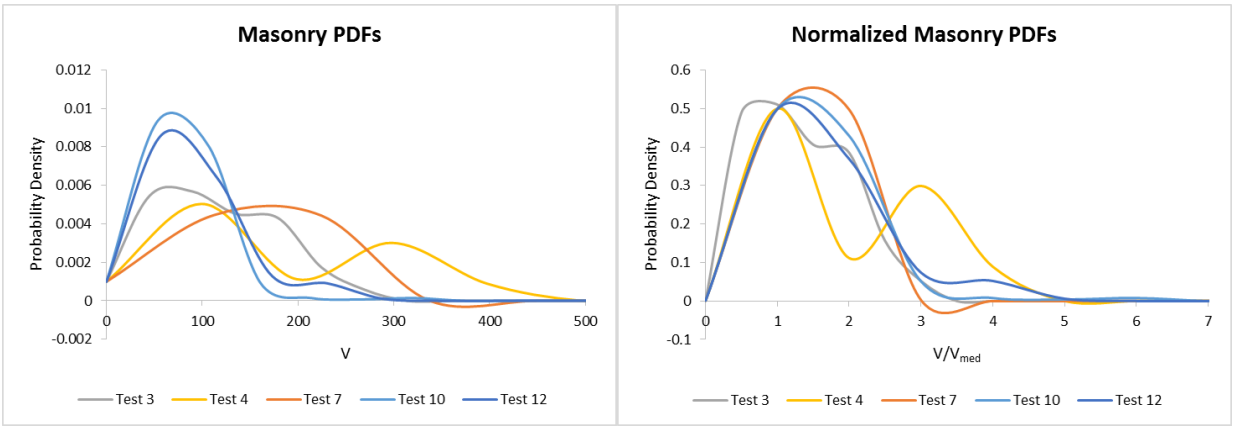


*a* *b*

**Figure 43.** Overlay of masonry test velocity data a) PDF and b) normalized by median mass

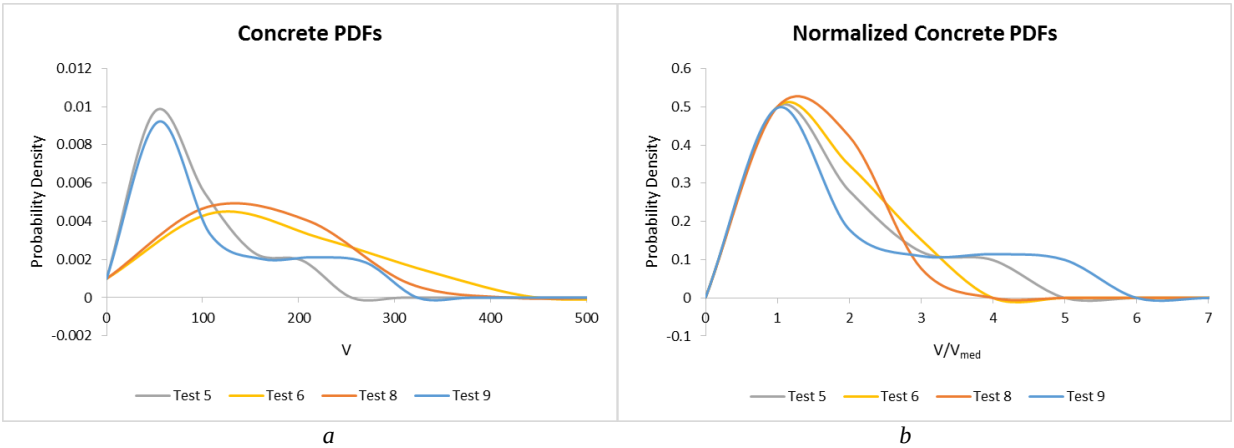


*a* *b*

**Figure 44.** Overlay of concrete test velocity data a) PDF and b) normalized by median mass

**DEPARTMENT OF DEFENSE**

DEFENSE THREAT REDUCTION
AGENCY
8725 JOHN J. KINGMAN ROAD
STOP 6201
FORT BELVOIR, VA 22060
ATTN: P. CLEMENT

DEFENSE TECHNICAL
INFORMATION CENTER
8725 JOHN J. KINGMAN ROAD,
SUITE 0944
FT. BELVOIR, VA 22060-6201
ATTN: DTIC/OCA

**DEPARTMENT OF DEFENSE CONTRACTORS**

QUANTERION SOLUTIONS, INC.
1680 TEXAS STREET, SE
KIRTLAND AFB, NM 87117-5669
ATTN: DTRIAC